

Feedback-induced desynchronization and oscillation quenching in a population of globally coupled oscillators

Ayumi Ozawa* and Hiroshi Kori

*Department of Complexity Science and Engineering,
The University of Tokyo, Chiba 277-8561, Japan*

(Dated: February 9, 2021)

Motivated from a wide range of applications, various methods to control synchronization in coupled oscillators have been proposed. Previous studies have demonstrated that global feedback typically induces three macroscopic behaviors: synchronization, desynchronization, and oscillation quenching. However, analyzing all of these transitions within a single theoretical framework is difficult, and thus the feedback effect is only partially understood in each framework. Herein, we analyze a model of globally coupled phase oscillators exposed to global feedback, which shows all of the typical macroscopic dynamical states. Analytical tractability of the model enables us to obtain detailed phase diagrams where transitions and bistabilities between different macroscopic states are identified. Additionally, we propose strategies to steer the oscillators into targeted states with minimal feedback strength. Our study provides a useful overview of the effect of global feedback and is expected to serve as a benchmark when more sophisticated feedback needs to be designed.

I. INTRODUCTION

Synchronization is a self-organization phenomenon that occurs in interacting oscillatory elements and is widely observed[1–5]. The resultant coherent oscillation is desirable in some systems. For example, synchronization is essential for the normal functioning of power grids [6]. Other beneficial effects of synchronization include the enhanced precision in biological oscillatory systems[4, 7–10], coordinated locomotion of animals and robots[11], and reduced congestion in models of traffic flow[12, 13].

However, synchronization may also cause problems. At the Millennium Footbridge in London, the steps of the pedestrians were synchronized, and considerable lateral movement of the bridge was observed[14]. Synchronization is also associated with neurological disorders. The local field potentials recorded from the brains of Parkinsonian patients and model animals often display marked oscillations, which are considered to be reflections of coherent neuronal activities[15]. Although

* ozawa-ayumi@g.ecc.u-tokyo.ac.jp

the mechanism of Parkinson’s disease is not well understood yet, exaggerated synchronization is one of the possible factors that induces related symptoms[16]. For some types of Parkinsonian patients, deep brain stimulation (DBS), which involves electrical stimulation to particular regions of the brain, may suppress the pathological collective oscillation and motor symptoms [15, 17]. However, this treatment is sometimes accompanied by negative side effects[18, 19]. Thus, milder ways of stimulation need to be developed.

The wide range of desirable and undesirable synchronization phenomena has drawn substantial research attention to the control of synchronization. As a control implementation, global feedback loops are known to be effective. In [20], the authors experimentally demonstrated that a synchronously oscillating state can be stabilized in a surface chemical reaction that inherently exhibits turbulent oscillatory dynamics. Global feedback may also desynchronize oscillator assemblies. Several types of mean-field feedback that efficiently desynchronize oscillators have been proposed [21–29]. Moreover, other behaviors may be realized through global feedback. It is proved that in a particular class of phase oscillators, the oscillation death state, in which the mean-field oscillation terminates, can be stabilized via global mean-field feedback [27]. Oscillation death is known to appear in various coupled oscillator systems [30].

These extensive studies [20–29] elucidated that global feedback typically stabilizes the synchronous, asynchronous, or oscillation-death states. However, in the oscillator models and feedback forms considered thus far, analytically treating all of these macroscopic states is difficult, and hence, a comprehensive phase diagram has not been obtained. With only partial knowledge being available on the phase diagram, feedback control may fail to realize a desired state owing to the unexpected stabilization of other states. Detailed phase diagrams of an analytically tractable model would provide an insight into a general principle of feedback control and help design and tune the feedback scheme.

Herein, we consider the Sakaguchi–Kuramoto model, which describes a population of nonidentical phase oscillators with global coupling, as a coupled-oscillator model and incorporate a global mean-field feedback loop into the system. We show that the system exhibits all three typical macroscopic states: the asynchronously oscillating state, the synchronously oscillating state, and the oscillation-death state. By invoking the Ott–Antonsen ansatz[31, 32], we comprehensively perform the existence and stability analysis of the macroscopic states, thus obtaining detailed phase diagrams in the space of feedback parameters for different coupling strengths. Our analysis elucidates (i) the dependency of the feedback effect on the parameters of the oscillator model; (ii) the optimal feedback parameters for stabilizing the asynchronous state with minimal feedback strength;

and (iii) the existence of the bistability between the oscillation-death state and one of the other two states. The obtained phase diagrams are numerically validated. In addition, we propose a strategy for realizing the asynchronous state in the bistable region. Finally, to support the robustness of our results, we numerically investigate another model that belongs to a more general class of oscillator models.

II. MODEL

We consider globally coupled phase oscillators under global feedback, given as

$$\frac{d\theta_i}{dt} = \tilde{\omega}_i + \frac{\tilde{K}}{N} \sum_{j=1}^N \sin(\theta_j - \theta_i + \beta) + \tilde{E} \sin(\theta_i + \alpha) F(\boldsymbol{\theta}), \quad (1)$$

where $\theta_i(\tilde{t})$ and $\tilde{\omega}_i$ ($i = 1, \dots, N$) represent the phase and natural frequency of the i th oscillator, respectively; $\tilde{K} \geq 0$ and $\tilde{E} \geq 0$ represent the strength of coupling and feedback, respectively; and α and β are parameters, which are usually nonvanishing in real oscillator systems[33, 34]. The function $F(\boldsymbol{\theta}) = F(\theta_1, \dots, \theta_N)$ describes a global feedback and $\sin(\theta_i + \alpha)$ is the phase sensitivity to the feedback. In particular, we consider

$$F(\boldsymbol{\theta}) = \frac{1}{N} \sum_{j=1}^N \cos(\theta_j - \delta), \quad (2)$$

$$= R \cos(\Theta - \delta), \quad (3)$$

where δ is a parameter referred to as the phase offset in the feedback, and $R = R(t)$ ($0 \leq R \leq 1$) and $\Theta = \Theta(t)$ ($0 \leq \Theta < 2\pi$) are the order parameter and mean phase defined by

$$r := R e^{i\Theta} = \frac{1}{N} \sum_{j=1}^N e^{i\theta_j}. \quad (4)$$

The R value indicates the synchronization level. The complex valued function $r = r(t)$ is referred to as the complex order parameter. Equation (1) reduces to the Kuramoto–Sakaguchi model[35] in the absence of feedback, i.e., for $\tilde{E} = 0$. See Appendix A for the derivation of Eq. (1) from a general class of coupled limit-cycle oscillators. As discussed in Appendix A, $F(\boldsymbol{\theta})$ corresponds to a linear function of mean fields in the limit-cycle model introduced in Appendix. A, and the parameters \tilde{E} and δ can be tuned to arbitrary values when two output signals are observed from individual oscillators. Alternatively, it can be implemented when $R(t)$ and $\Theta(t)$ are inferred online.

For analytical tractability, we assume $\tilde{\omega}_i$ to be drawn from the Lorentzian distribution $\tilde{g}(\tilde{\omega}) = \frac{\tilde{\gamma}}{\pi} \frac{1}{(\tilde{\omega} - \omega_0)^2 + \tilde{\gamma}^2}$, where $\tilde{\gamma} > 0$ and $\omega_0 > 0$. Without loss of generality, we decrease the number of

parameters by introducing nondimensional quantities $t = \omega_0 \tilde{t}$, $\gamma = \frac{\tilde{\gamma}}{\omega_0}$, $K = \frac{\tilde{K}}{\omega_0}$, $E = \frac{\tilde{E}}{\omega_0}$, and further replacing $\theta_i + \alpha$ by θ_i for $i = 1, \dots, N$ and $\delta + \alpha$ by δ . The resultant equation is

$$\frac{d\theta_i}{dt} = \omega_i + \frac{K}{N} \sum_{j=1}^N \sin(\theta_j - \theta_i + \beta) + E \sin \theta_i F(\boldsymbol{\theta}), \quad (5)$$

or

$$\dot{\theta}_i = \omega_i + KR \sin(\Theta - \theta_i + \beta) + ER \cos(\Theta - \delta) \sin \theta_i, \quad (6)$$

where ω_i is drawn from

$$g(\omega) = \frac{\gamma}{\pi} \frac{1}{(\omega - 1)^2 + \gamma^2}. \quad (7)$$

Now, the mean frequency is set to unity. Equation (6) with Eqs. (2) and (7) is analyzed below.

There are six parameters involved: $N, K > 0, E > 0, \beta, \delta$, and γ .

It is known that for $N \rightarrow \infty$, a certain class of oscillator assemblies including Eq. (6) has a low-dimensional manifold, on which a reduced dynamical equation can be obtained [31, 32]. By following [36], we obtain a closed equation for r on the manifold, given as

$$\dot{r} = \left(-\gamma + \frac{K e^{i\beta}}{2} + i \right) r - \frac{K e^{-i\beta}}{2} |r|^2 r - \frac{ER \cos(\Theta - \delta)}{2} (1 - r^2). \quad (8)$$

Here, we redefined $r = R e^{i\Theta}$ as its continuous analogue

$$r = \iint \rho(\theta, \omega, t) e^{i\theta} d\theta d\omega, \quad (9)$$

where $\rho(\theta, \omega, t) d\theta d\omega$ is the fraction of the oscillators with natural frequencies between ω and $\omega + d\omega$ and phases between θ and $\theta + d\theta$ at time t . For finite but sufficiently large N , Eq. (8) is expected to appropriately approximate the behavior of $r(t)$ in Eq. (6) after a transient time.

Henceforth, we assume $|\beta| < \pi/2$; the coupling promotes synchronization.

III. EFFECT OF FEEDBACK ON THE MACROSCOPIC STATE

A. Classification of macroscopic states

Dynamical properties of the system described by Eq. (8) in the absence of feedback ($E = 0$) are evident. This system always has a global attractor for any parameter values within $K \geq 0$ and $-\frac{\pi}{2} < \beta < \frac{\pi}{2}$. There are two global attractors: the steady solution $r(t) = 0$ for $K \leq K_c$ and the limit cycle solution $r(t) = r_0 e^{i\tilde{\omega}t}$ for $K > K_c$, where $K_c = 2\gamma / \cos \beta$, $r_0 = [1 - K_c/K]^{1/2}$, and

$\tilde{\omega} = 1 + K \sin \beta - \gamma \tan \beta$. The former corresponds to the asynchronous state, where the oscillators rotate with their natural frequencies. The latter corresponds to the synchronously oscillating state, where a subpopulation of the oscillators is phase-locked to the oscillating mean field. Figure 1 (a–c) shows typical dynamics of Eq. (6) for $E = 0$.

In addition to these two attractors, a stable steady solution $r(t) = r^* \neq 0$ may arise in the presence of the feedback ($E > 0$). We refer to the macroscopic state corresponding to this solution as the oscillation-death state because of the cessation of the microscopic and macroscopic oscillations explained below. To understand the dynamics of individual oscillators in the oscillation-death state ($r(t) = r^*$), let us consider Eq. (6). Inserting $r^* = R^* e^{i\Theta^*}$ into Eq. (6), we obtain

$$\dot{\theta}_i = \omega_i + A \sin(\theta_i + B), \quad (10)$$

where

$$A = R^* [(E \cos(\Theta^* - \delta) - K \cos(\Theta^* + \beta))^2 + (K \sin(\Theta^* + \beta))^2]^{1/2}, \quad (11)$$

$$\tan B = \frac{K \sin(\Theta^* + \beta)}{E \cos(\Theta^* - \delta) - K \cos(\Theta^* + \beta)}. \quad (12)$$

A stable fixed point of Eq. (10) exists for $|\omega_i| < |A|$, which implies that the oscillators with $|\omega_i| < |A|$ cease their oscillations. Thus, the solution $r(t) = r^* \neq 0$ corresponds to the oscillation-death state, where a subpopulation of the oscillators and the mean field quit oscillations. Figure 1(d) and the blue dotted line in Fig. 1(a) exemplify the dynamics of the oscillators and the order parameter, respectively, in the oscillation-death state.

B. Bifurcation analysis and phase diagrams

The following bifurcation analysis of Eq. (8) enables us to obtain the phase diagrams shown in Fig. 2.

First, we analyze the bifurcation of the fixed point $r = 0$, i.e., the asynchronous state. Substituting $r = x + iy$ ($x, y \in \mathbb{R}$) into Eq. (8) and linearizing the equations for dx/dt and dy/dt around $(x, y) = (0, 0)$, we obtain the stability matrix

$$L = \begin{bmatrix} \Lambda - \frac{E}{2} \cos \delta & -\Omega - \frac{E}{2} \sin \delta \\ \Omega & \Lambda \end{bmatrix}, \quad (13)$$

where $\Lambda = -\gamma + \frac{K}{2} \cos \beta$ and $\Omega = 1 + \frac{K}{2} \sin \beta$. The quantity Ω represents the frequency of collective oscillation at its onset, i.e., at $K = K_c$, in the absence of feedback.

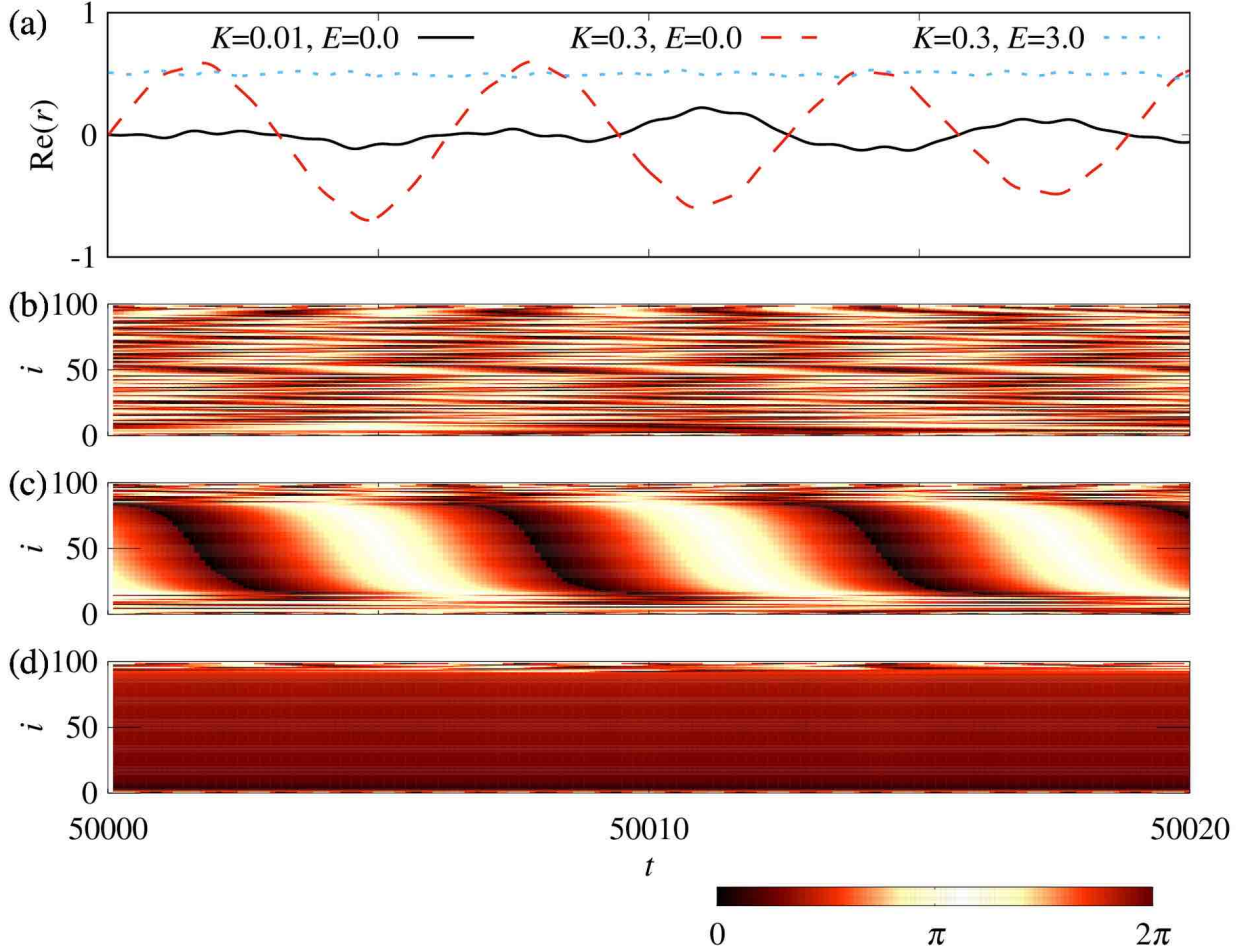


FIG. 1. (Color online) Three types of macroscopic state of the $N = 100$ oscillators described by Eq. (6). (a) Time series of the real part of the complex order parameter r for different parameter regimes. The black solid, red dashed, and blue dotted lines represent the solutions corresponding to the asynchronously oscillating state, the synchronously oscillating state, and the oscillation-death state, respectively. The coupling strength and feedback parameters are set to $K = 0.01$ and $E = \delta = 0$ (solid black line), $K = 0.3$ and $E = \delta = 0$ (red dashed line), and $K = 0.3$, $E = 3.0$, and $\delta = -\pi/3$ (blue dotted line). The other parameters are $\gamma = 0.1$ and $\beta = 0$. (b)–(d) Time series of the individual oscillators. The vertical axis is the index of the oscillator, and the color scale represents its phase. The natural frequency ω_i is set to be monotonically increasing with the oscillator index i : $\omega_i = 1 + \gamma \tan \left[\frac{i\pi}{N} - \frac{(N+1)\pi}{2N} \right]$. The parameters for (b), (c), and (d) are identical to those of the black solid, red dashed, and blue dotted lines in Fig. 1(a), respectively.

The saddle-node, transcritical, pitchfork, and Hopf bifurcations are the codimension-one bifurcations that alter the local stability and/or number of fixed points. The first three bifurcations occur when one of the eigenvalues of the stability matrix vanishes, which can be captured by its necessary condition $|L| = 0$. Hopf bifurcation occurs when both eigenvalues of L become purely

imaginary, i.e., $\text{Tr } L = 0$ and $|L| > 0$.

Solving $\text{Tr } L = 0$ for E under the condition $|L| > 0$ yields the Hopf bifurcation curve

$$E_{\text{hopf}} = \frac{4\Lambda}{\cos \delta}, \quad (14)$$

where δ satisfies

$$-\Lambda^2 + \Omega^2 + 2\Lambda\Omega \tan \delta > 0. \quad (15)$$

The curve defined by Eqs. (14) and (15) is depicted by the orange dashed line in Fig.2(a)–(c). Because $\text{Tr } L = 2\Lambda(1 - E/E_{\text{hopf}})$, the asynchronous state is unstable for $E < E_{\text{hopf}}$ (resp. $E > E_{\text{hopf}}$) when $\Lambda > 0$ (resp. $\Lambda < 0$). The bifurcation is revealed to be supercritical by the weakly nonlinear analysis performed in Appendix C. Therefore, a continuous transition between the asynchronous and synchronous states occurs on this curve.

The condition $|L| = 0$ yields another bifurcation curve:

$$E_{\text{pf}} = \frac{2(\Lambda^2 + \Omega^2)}{\Lambda \cos \delta - \Omega \sin \delta}. \quad (16)$$

On this curve, the pitchfork bifurcation occurs because Eq. (8) is invariant under the change of $r \rightarrow -r$. See Appendix B for the transformation of Eq. (8) to a normal form and for a brief explanation on why this bifurcation cannot be a transcritical or saddle-node bifurcation. Because $|L|$ can be described as $|L| = (\Lambda^2 + \Omega^2)(1 - E/E_{\text{pf}})$, the asynchronous state is unstable for $E > E_{\text{pf}}$ when $\Lambda\Omega \neq 0$. The stability of a fixed point changes through this bifurcation if the non-zero eigenvalue of the stability matrix is negative; i.e., $\text{Tr } L < 0$, or

$$2\Lambda < \frac{\Lambda^2 + \Omega^2}{\Lambda - \Omega \tan \delta}. \quad (17)$$

The curve defined by Eqs. (16) and (17) is highlighted using magenta solid line labeled as PFs in Fig. 2. On this bifurcation curve, the asynchronous state loses its stability. Moreover, weakly nonlinear analysis performed in Appendix B implies that this bifurcation is subcritical in the parameter region considered in Fig. 2. This suggests the existence of the bistability between the asynchronous and oscillation-death states near the curve, which will be numerically confirmed in Sec. III C.

The pitchfork bifurcation occurs to an unstable fixed point if the non-zero eigenvalue of the stability matrix on the bifurcation curve is positive; i.e., $\text{Tr } L > 0$. We thus obtain the curve for this bifurcation, which is defined by Eq. (16) and Eq. (17) but with the opposite inequality. The obtained curve is shown by the dot-dashed line labeled as PFu in Fig. 2. Because no stable state emerges with this bifurcation, the curve is not relevant to the phase diagram.

Next, we investigate the bifurcation of the fixed point $r^* \neq 0$, i.e., the oscillation-death state.

For convenience, we express Eq. (8) using polar coordinates:

$$\frac{dR}{dt} = R \left\{ -\gamma + (1 - R^2) \left[\frac{K}{2} \cos \beta - \frac{E}{4} (\cos(\delta - 2\Theta) + \cos \delta) \right] \right\} \quad (18a)$$

$$\frac{d\Theta}{dt} = 1 + (1 + R^2) \left[\frac{K}{2} \sin \beta + \frac{E}{4} (\sin \delta - \sin(\delta - 2\Theta)) \right]. \quad (18b)$$

A fixed point $r^* = R^* e^{i\Theta^*}$ is given as a solution to $dR/dt = 0$ and $d\Theta/dt = 0$; however, this is difficult to solve explicitly. Nevertheless, we can still obtain the stability matrix by linearizing Eq. (18) around $(R, \Theta) = (R^*, \Theta^*)$, as

$$M = \begin{bmatrix} -\frac{2R^{*2}\gamma}{1-R^{*2}} & -\frac{E}{2} R^* (1 - R^{*2}) \sin(\delta - 2\Theta^*) \\ -\frac{2R^*}{R^{*2}+1} & \frac{E}{2} (R^{*2} + 1) \cos(\delta - 2\Theta^*) \end{bmatrix}. \quad (19)$$

Below, we show that the bifurcation curve can be obtained as a function of R^* and drawn in the phase diagram by varying R^* in the range of $0 < R^* < 1$.

By solving $|M| = 0$ and using the identity $\sin^2(\delta - 2\Theta^*) + \cos^2(\delta - 2\Theta^*) = 1$, we obtain

$$\sin(\delta - 2\Theta^*) = \pm \frac{1}{\sqrt{1 + \xi^2}}, \quad (20a)$$

$$\cos(\delta - 2\Theta^*) = \mp \frac{\xi}{\sqrt{1 + \xi^2}}, \quad (20b)$$

where

$$\xi = \frac{(R^{*2} - 1)^2}{\gamma (R^{*2} + 1)^2}. \quad (21)$$

By substituting Eq. (20) into Eq. (18) and inserting $dR/dt = d\Theta/dt = 0$, we obtain

$$E = \pm \frac{\sqrt{\xi^2 + 1} \left((2\gamma + KQ_- \cos \beta)^2 + \gamma \xi (KQ_+ \sin \beta + 2)^2 \right)}{\xi (4\gamma - KQ_-^2 \cos \beta + \gamma KQ_+^2 \sin \beta)}, \quad (22a)$$

$$\cos \delta = \pm \frac{2\xi(2\gamma + KQ_- \cos \beta) (4\gamma - KQ_-^2 \cos \beta + \gamma KQ_+^2 \sin \beta)}{\sqrt{\xi^2 + 1} Q_- \left((2\gamma + KQ_- \cos \beta)^2 + \gamma \xi (KQ_+ \sin \beta + 2)^2 \right)} \pm \frac{\xi}{\sqrt{\xi^2 + 1}}, \quad (22b)$$

$$\sin \delta = \mp \frac{2\xi(KQ_+ \sin \beta + 2) (4\gamma - KQ_-^2 \cos \beta + \gamma KQ_+^2 \sin \beta)}{\sqrt{\xi^2 + 1} Q_+ \left((2\gamma + KQ_- \cos \beta)^2 + \gamma \xi (KQ_+ \sin \beta + 2)^2 \right)} \pm \frac{1}{\sqrt{\xi^2 + 1}}, \quad (22c)$$

where $Q_+ = 1 + R^{*2}$ and $Q_- = -1 + R^{*2}$. Inserting $0 < R < 1$ into Eq. (22) yields the cyan dotted curve in Fig. 2. As rationalized below, this curve represents the saddle-node bifurcation at which stable and unstable oscillation death solutions that exist in the area surrounded by the curve collide and disappear. If transcritical or pitchfork bifurcation occurred on the curve, there should be a fixed point $r^* \neq 0$ below the curve. Such a fixed point may not disappear unless a bifurcation involving that point occurs, thus it should persist up to the parameter region of $E = 0$.

However, this contradicts the fact that no isolated fixed point except $r = 0$ exists at $E = 0$. Thus, a saddle–node bifurcation occurs on the curve. We now know that a pair of fixed points arise through the bifurcation, but their stability remains unclear. Expressing $\text{Tr } M$ as a function of R^* , we numerically confirmed that $\text{Tr } M < 0$ holds on the bifurcation curve. This implies that a stable node and a saddle collide on the bifurcation curve. Therefore, we conclude that a stable oscillation–death state exists inside the curve and disappears on the curve.

It is useful to obtain an approximate expression for the saddle–node bifurcation as a function of δ . To this end, for some parameter regions, we derive a necessary condition and a sufficient condition for a nonzero fixed point (R^*, Θ^*) to exist. If a nonzero fixed point (R^*, Θ^*) exists, it must satisfy $d\Theta/dt|_{\Theta=\Theta^*} = 0$, or,

$$E = \frac{4 + 2K(1 + R^{*2}) \sin \beta}{(1 + R^{*2})(\sin(\delta - 2\Theta^*) - \sin \delta)}. \quad (23)$$

The numerator on the right-hand side is positive when $\Omega' := 1 + K \sin \beta > 0$. In this case, a lower bound $E_{\text{lower}} \leq E$ is given by Eq. (23) with $R^{*2} = 1$ and $\sin(\delta - 2\Theta^*) = 1$, i.e.,

$$E_{\text{lower}} = \frac{2\Omega'}{1 - \sin \delta}. \quad (24)$$

Thus, when $\Omega' > 0$, a necessary condition for the existence of a nonzero fixed point is given by

$$E \geq E_{\text{lower}}. \quad (25)$$

Next, we address a sufficient condition for the existence of a nonzero fixed point. We restrict ourselves to the parameter region where $\Omega' > 0$ and $K > 2K_c$ holds. Then, for the parameter region under consideration, as shown in Appendix D, a nonzero fixed point exists if E satisfies both of the following inequalities:

$$E > E_{\text{lower}} (1 + \eta) \quad (26)$$

and

$$E < \frac{K \cos \beta}{1 + \cos \delta}, \quad (27)$$

where

$$\eta = \frac{K_c/K}{(2 - K_c/K)(1 + K \sin \beta)}. \quad (28)$$

We can find such E for $\beta \simeq 0$ and sufficiently large K when a value of δ is given. See Appendix D for details.

From Eq. (25) and (26), for $\Omega' > 0$, $\beta \simeq 0$, and sufficiently large K , it follows that the saddle–node bifurcation should occur at $E \in [E_{\text{lower}}, E_{\text{lower}}(1 + \eta)]$. As $\eta \rightarrow 0$ as $K \rightarrow \infty$, the bifurcation curve is well approximated by E_{lower} for large K . In Fig. 2(c), we observe that E_{lower} , which is depicted as the approximate SN (aSN) curve, approximates the saddle–node bifurcation curve well, although the sufficient condition given by Eqs. (26) and (27) cannot be satisfied in a range of δ .

Similarly to the saddle–node bifurcation curve, the Hopf bifurcation curve is obtained by imposing $\text{Tr } M = 0$ and $|M| > 0$. The former condition yields

$$E = \sqrt{\frac{[Q_-^2 s^2 + (c + 2\gamma(2R^{*2} + 1))^2 - 4\gamma^2 R^{*4}]^2}{Q_+^2 Q_-^4 s^2}} + \frac{16\gamma^2 R^{*4}}{Q_+^2 Q_-^2}, \quad (29a)$$

$$\cos \delta = \frac{2(c + 2\gamma(2R^{*2} + 1))}{EQ_+ Q_-}, \quad (29b)$$

$$\sin \delta = -\frac{2s}{EQ_+} - \sqrt{1 - \frac{16\gamma^2 R^{*4}}{E^2 Q_+^2 Q_-^2}}, \quad (29c)$$

where

$$(c + 2\gamma(2R^{*2} + 1))^2 - 4\gamma^2 R^{*4} + s^2 Q_-^2 \leq 0, \quad (30)$$

$$s = K(1 + R^{*2}) \sin \beta + 2, \quad (31)$$

$$c = K(-1 + R^{*4}) \cos \beta. \quad (32)$$

Inserting $0 < R^* < 1$ into Eqs. (29a), (29b), and (29c) and requiring $|M| > 0$ and Eq. (30) on the curve, we obtain the Hopf bifurcation curve. As shown in Appendix E, Hopf bifurcation may also occur; however, this is not the case for the parameter region considered in Fig. 2.

A codimension-two bifurcation occurs at which the curves PFs and PFu meet. A normal form of this bifurcation is known [37]. The weakly nonlinear analysis of our system performed in Appendix E implies that for $\Omega > 0$, a heteroclinic bifurcation curve extends from this point. The navy solid curve labeled by HC shows the heteroclinic bifurcation curve obtained using the software XPPAUT[38].

Figure 2 indicates that the heteroclinic bifurcation curve ends up at a point on the saddle–node bifurcation curve, where another codimension-two bifurcation should occur. The observation of vector fields around this bifurcation point, shown in Fig. 3, reveals that the saddle–node bifurcation curve is subdivided into two parts at this point, and the one labeled by SNIC in Fig. 2 corresponds to saddle–node bifurcation on an invariant circle. A very similar codimension-two bifurcation is reported in [39], where SN, SNIC, and homoclinic bifurcation curves meet. We obtain a heteroclinic

bifurcation curve rather than a homoclinic one because of the invariance of our system under $r \rightarrow -r$.

The three bifurcation curves HB, HC, and SNIC in Fig. 2 form the boundary of the stable synchronous state, provided that there is no other bifurcation involving periodic solutions, such as the saddle–node bifurcation of limit cycles. Then, the bistable region exists in the area surrounded by PFs, HC, and SN. Altogether, we obtain three qualitatively different phase diagrams depending on K values, as shown in Fig. 2. Our extensive numerical analysis performed in Sec. III C and Appendix F indicates that the phase diagrams given in Fig. 2 are comprehensive.

Other bifurcations may occur typically for $\Omega < 0$. As briefly mentioned in Appendix E, the codimension-two bifurcation at the intersection of Hopf, PFs, and PFu has a topologically different structure for $\Omega < 0$. The situation $\Omega < 0$ occurs for $-\frac{\pi}{2} < \beta < 0$ and sufficiently large K . In such a situation, in the absence of feedback, the mean field oscillates with a frequency opposite to that of the typical natural frequency of individual oscillators, i.e., $\omega_0 = 1$. This implies that synchronized individual oscillators also have frequencies opposite to their natural ones. However, such a phenomenon is not commonly observed in limit-cycle oscillators and should be regarded as an artifact owing to the use of phase approximation for a case of strong coupling. We therefore omit the case of $\Omega < 0$ in the present paper.

C. Numerical verification

To verify the the analyses in Sec. III B, we simulated Eq. (6) for $N = 2000$. We set $\omega_i = \omega_0 + \gamma \tan \left[\frac{i\pi}{N} - \frac{(N+1)\pi}{2N} \right]$ with $\omega_0 = 1$, which converges to the Lorentzian distribution at $N \rightarrow \infty$ [40]. In Fig. 4(a) and its magnifications Fig. 4(b) and (c), we show the value of $\langle R \rangle$ for different feedback parameters, where the angle brackets denote the long-time average. As the initial condition, we employ the uniform state, i.e., $\theta_i(0) = 2\pi(i-1)/N$ for $i = 1, \dots, N$, in Fig. 4(a,b) and the fully synchronized state, i.e., $\theta_i(0) = 0$ for $i = 1, \dots, N$, in Fig. 4(c). The parameters are same as in Fig. 2(b), and we draw the same bifurcation curves in Fig. 4(a–c) for comparison.

In the black regions in Fig. 4, $\langle R \rangle \simeq 0$ is obtained, which indicates that the system is in the asynchronous state. Because the initial condition employed in Fig. 4(a,b) is considered to be very close to the asynchronous state, the asynchronous state should be locally stable in the black region in Fig. 4(a,b), which is in excellent agreement with our prediction in Fig. 2(b).

Moreover, we can observe a discrepancy between Figs. 4(b) and (c) in the region surrounded by the curves SN, HB, and PFs, where the bistability between the asynchronous and oscillation-

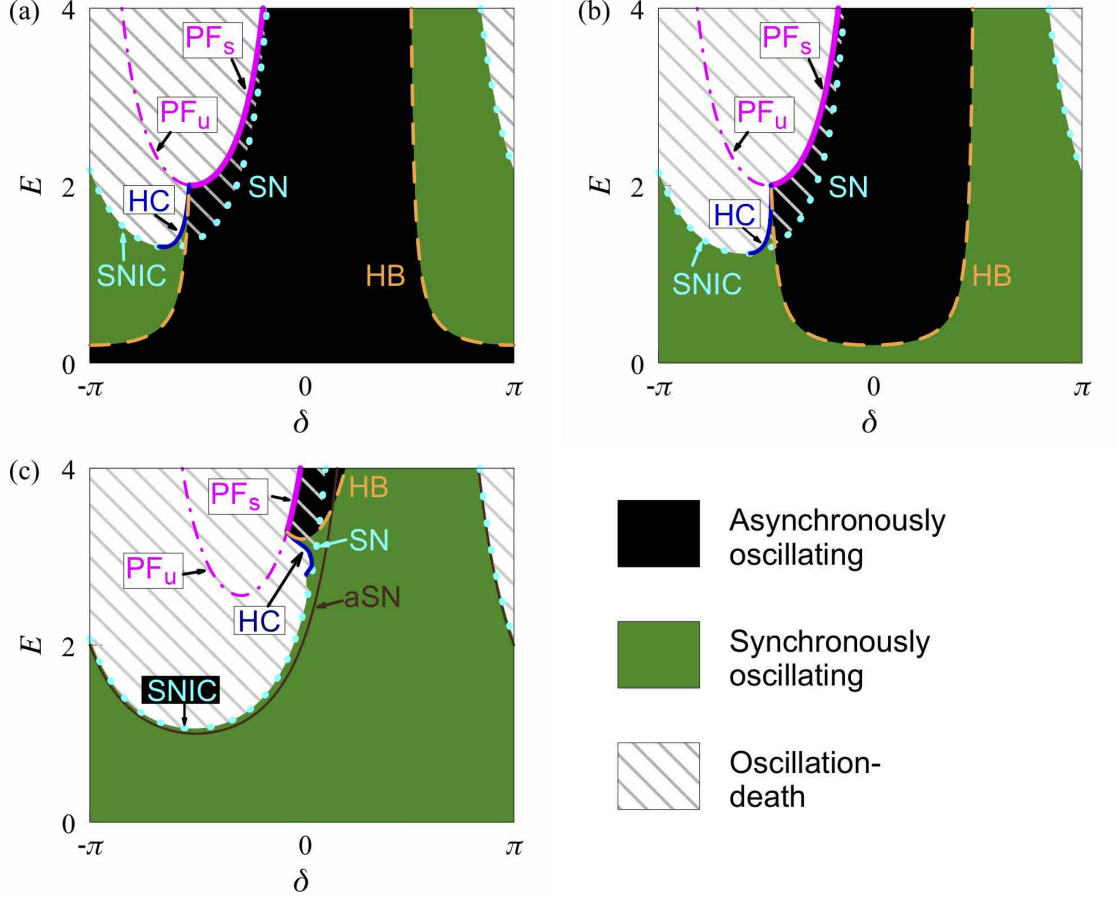


FIG. 2. (Color online) Phase diagrams of the macroscopic state based on the stable solutions of Eq.(8) for (a) $K = 0.1 < K_c$, (b) $K = 0.3 > K_c$, and (c) $K = 1.8 \gg K_c$, where $K_c = 2\gamma / \cos \beta = 0.2$. Other parameters are $\gamma = 0.1$ and $\beta = 0$. The black, green, and shaded regions correspond to the asynchronous, synchronously oscillating, and oscillation-death states, respectively.

death states is predicted. To clarify which region of nonvanishing $\langle R \rangle$ in Fig. 2 corresponds to the synchronously oscillating or oscillation-death states, we further measure $\langle \zeta \rangle$, where $\zeta = |r - \langle r \rangle|$. From the definition of R and ζ , $\langle R \rangle > 0$ and $\langle \zeta \rangle = 0$ imply that the system is in the oscillation-death state, thus we confirm the predicted bistability as well as the existence of the stable oscillation-death state inside the SN and SNIC curves.

IV. OPTIMAL FEEDBACK PARAMETERS

We consider $K > K_c$, or equivalently $\Lambda := -\gamma + \frac{K}{2} \cos \beta > 0$, for which the system falls into the synchronously oscillating state in the absence of the feedback, and determine the value of the phase offset δ that minimizes the required feedback strength E to suppress the synchronized

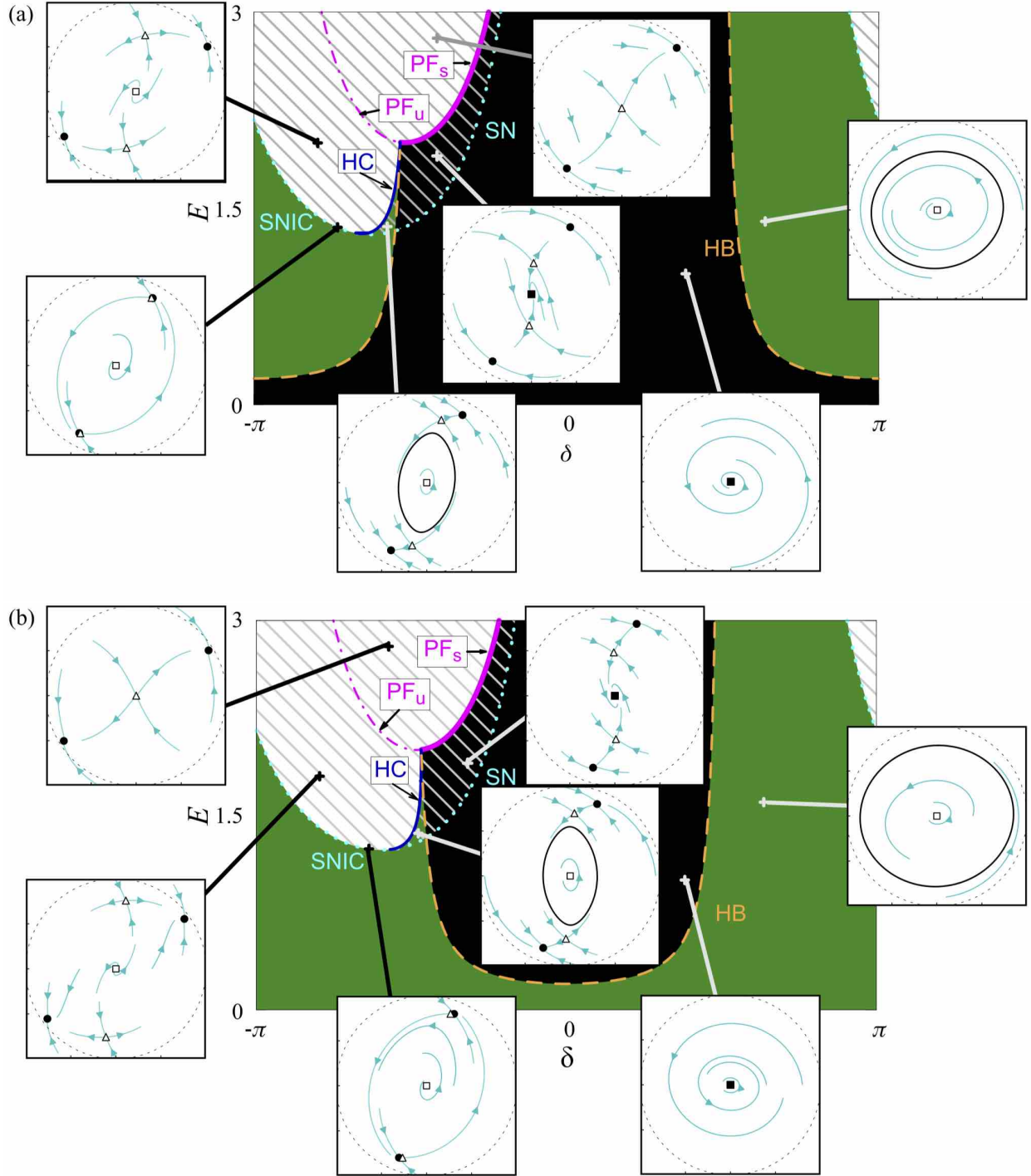


FIG. 3. (Color online) Typical vector fields of Eq. (8) for different areas of the phase diagrams in Fig. 2. The vector fields on the complex planes are drawn with cyan arrows. Filled (resp. open) squares represent stable (resp. unstable) spirals, and filled (resp. open) circles represent stable (resp. unstable) nodes. The open triangles represent saddles. Stable limit cycles are illustrated using black solid curves. The circle drawn with the dashed line on each panel depicts the unit circle on the complex plane. The parameters for (a) and (b) are the same as those shown in Fig. 2(a) and (b), respectively.

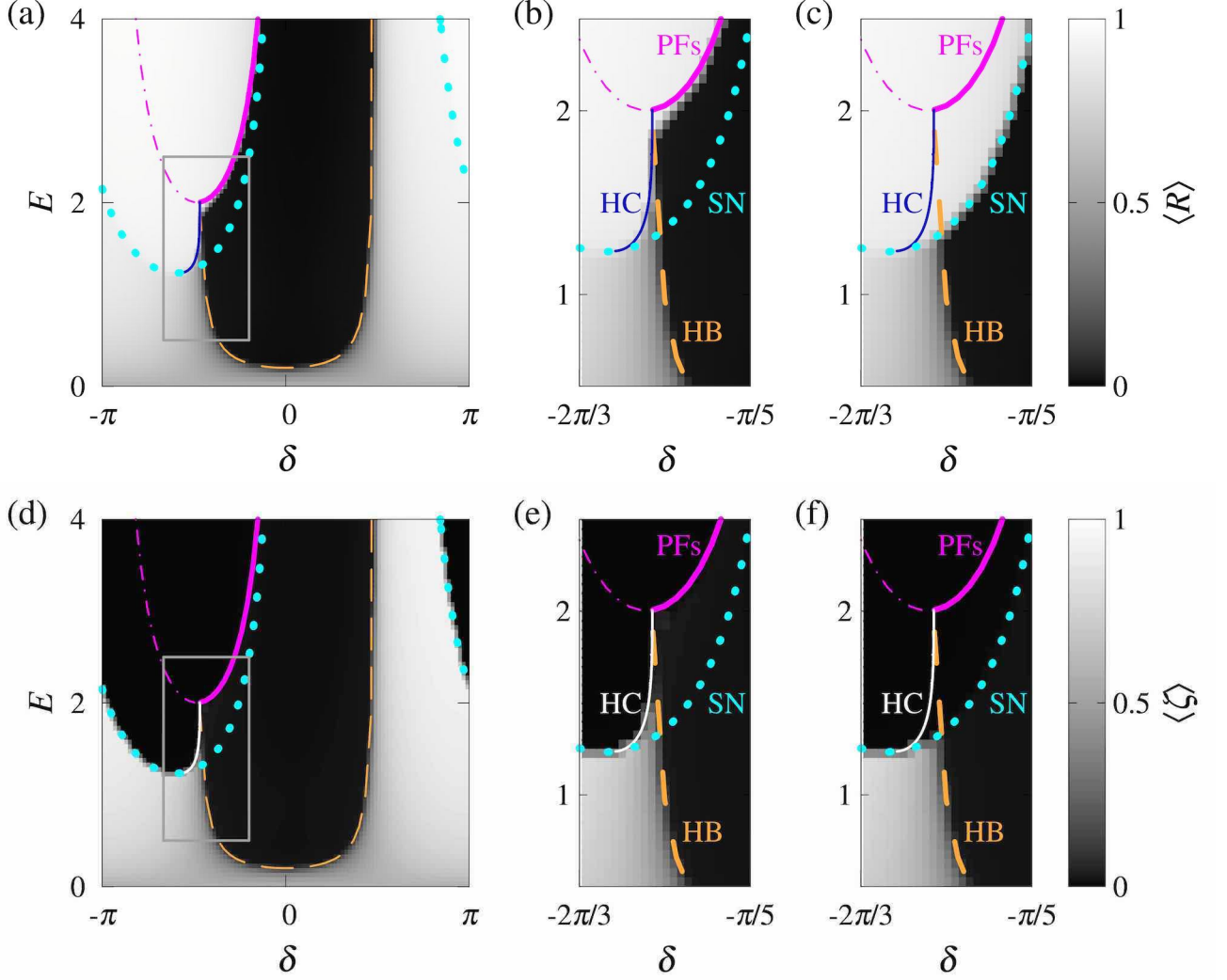


FIG. 4. (Color online) Simulation results of Eq. (6). Long-time average of (a–c) R and (d–f) ζ . Parameters are the same as those in Fig. 2(b), and the same bifurcation curves are drawn here. The parameter range in (b,c,e,f) is the same as that in the boxed area in (a,d). The initial condition is the uniform phase distribution in (a,b,d,e) and the fully synchronized state in (c,f).

oscillations. We can achieve this by leading the system to (i) the asynchronous state and (ii) the oscillation-death state. Their optimal parameter sets (δ, E) are denoted by (i) $(\delta_{\text{async}}, E_{\text{async}})$ and (ii) $(\delta_{\text{death}}, E_{\text{death}})$.

The point $(\delta_{\text{async}}, E_{\text{async}})$ can be determined analytically. Because the asynchronous state is stable for E above the HB curve and below the PFs curve, $(\delta_{\text{async}}, E_{\text{async}})$ is given by the minimum

of the HB curve. Further, $\delta = 0$ provides the minimum when Eq. (15) holds for $\delta = 0$, resulting in

$$\delta_{\text{async}} = 0, \quad (33a)$$

$$E_{\text{async}} = 4\Lambda = -4\gamma + 2K \cos \beta. \quad (33b)$$

This is the case when $\Lambda \leq |\Omega| = |1 + \frac{K}{2} \sin \beta|$, which typically arises for small K or large $\tan \beta$. For $\Lambda > |\Omega|$, the smallest $|\delta|$ that satisfies Eq. (15) provides the minimum; i.e.,

$$\delta_{\text{async}} = \frac{\Omega}{|\Omega|} \arcsin \left(\frac{\Lambda^2 - \Omega^2}{\Lambda^2 + \Omega^2} \right), \quad (34a)$$

$$E_{\text{async}} = \frac{2(\Lambda^2 + \Omega^2)}{|\Omega|}. \quad (34b)$$

Although $(\delta_{\text{death}}, E_{\text{death}})$ can only be numerically determined using Eqs. (22) and (29), an approximate expression can be obtained from (24):

$$\delta_{\text{death}} \approx -\frac{\pi}{2}, \quad (35a)$$

$$E_{\text{death}} \approx 1 + K \sin \beta. \quad (35b)$$

Figure 5 shows the parameter-dependency of E_{async} given by Eqs. (33b) and (34b) and E_{death} obtained numerically using Eqs. (22) and (29). The general tendency is well captured by Eqs. (33b) and (35b). The solid lines represent the parameter set at which $E_{\text{async}} = E_{\text{death}}$. Based on Eqs. (33b) and (35b), we can roughly estimate that the asynchronous (oscillation-death) state can be achieved with a smaller feedback strength when $-4\gamma + 2K \cos \beta$ is small (large) compared to $1 + K \sin \beta$.

When we desire to suppress the collective oscillation without causing oscillation death, we need to consider the bistability between the asynchronous and oscillation-death states. For example, see Fig. 2(c), where $\delta_{\text{async}} = 0$. Suppose that we increase E while fixing $\delta = 0$. Then, the oscillation-death state will be obtained before the asynchronous state. By further increasing E , we will eventually arrive at the HB curve, above which the asynchronous state is stable. However, because of the bistability, the oscillation-death state is expected to be sustained even in that region. Therefore, to realize the asynchronous state, we need to use a larger δ value at which we first arrive at the monostable region of the asynchronous state. Once the asynchronous state is realized, we can vary δ to $\delta = 0$ and decrease E to E_{async} . To keep E as small as possible during the whole manipulation, we should employ a δ value close to that of the intersection of the HB and SN curves. Using the HB curve given by (14) and aSN curve given by Eq. (24), the approximate intersection

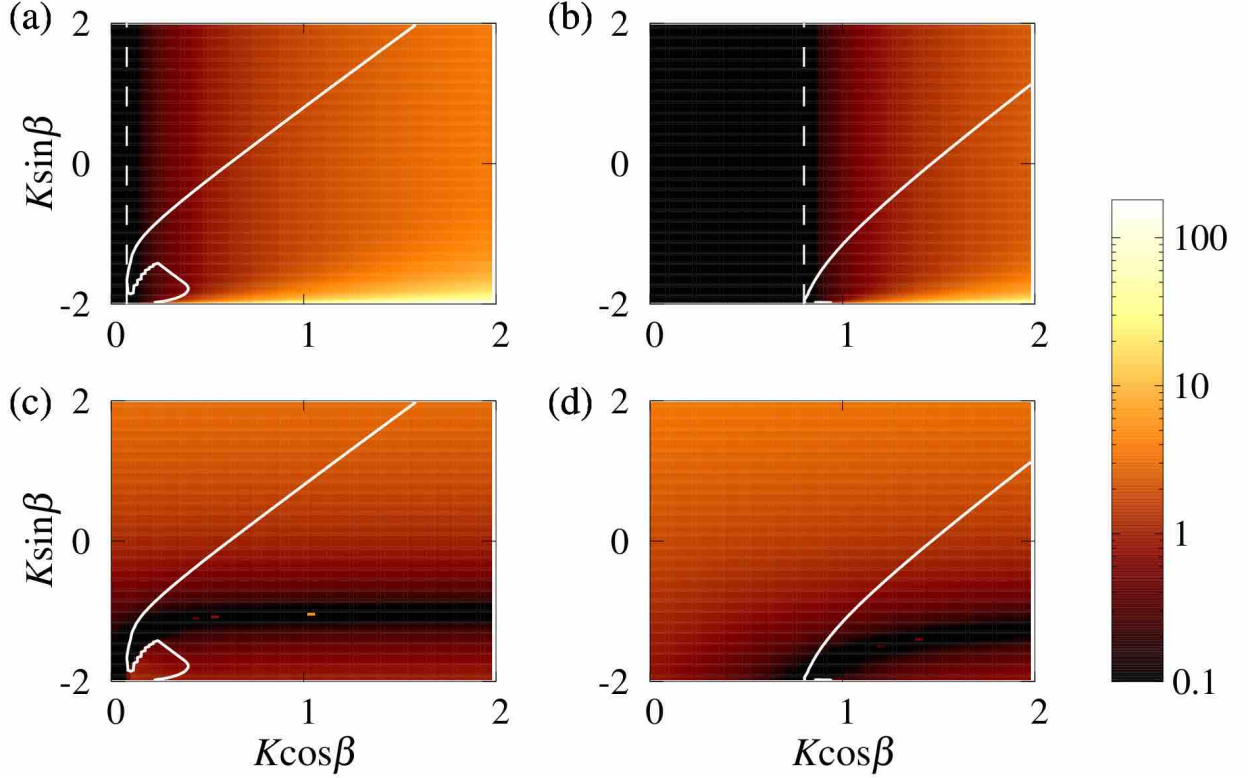


FIG. 5. (Color online) Parameter dependency of (a,b) E_{async} and (c,d) E_{death} . The solid lines represents the parameter values at which $E_{\text{death}} = E_{\text{async}}$ holds. (a,c) $\gamma = 0.04$. (b,d) $\gamma = 0.4$. On the left side of the dashed lines in (a) and (b), which depict $K \cos \beta = 2\gamma$, we have $E_{\text{async}} = 0$ because the solution $r = 0$ is stable even without feedback.

can be found as

$$(\delta, E) \approx \left(\frac{\pi}{2} - 2\alpha, \frac{\Omega'^2 + 4\Lambda^2}{\Omega'^2} \right), \quad (36)$$

where

$$\alpha = \arcsin \left[\frac{\Omega'}{\sqrt{\Omega'^2 + 4\Lambda^2}} \right]. \quad (37)$$

Using this δ value, we can efficiently steer the system into the asynchronous state.

Note that in contrast to the case of the stabilization of the asynchronous state, the feedback does not vanish when the oscillation-death state is achieved. Moreover, the minimum value of E does not necessarily imply that the intensity of the feedback $|Ef(r)|$ is minimized as it also depends on r . Instead, this optimization does minimize the possible feedback intensity

We perform numerical simulations of Eq. (6) to verify whether a near-optimal feedback properly works. Figure 6 shows the time-series of the collective oscillation $\text{Re}(r(t))$ and the individual phases

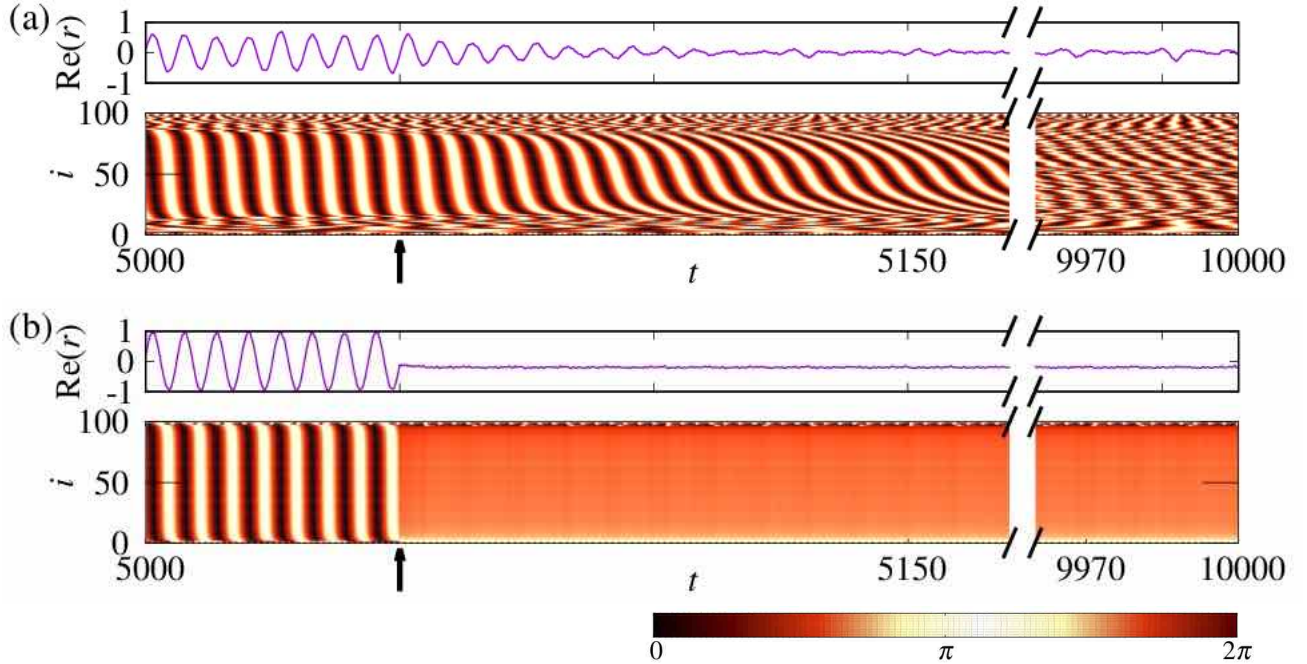


FIG. 6. (Color online) Alteration of the dynamics of the $N = 100$ oscillators by the feedback. In each figure, the upper panel displays the time series of $\text{Re}(r)$ while the lower panel shows the phases of the oscillators. (a) The feedback parameters are set as $E = 0.3 \approx E_{\text{asynch}}$ and $\delta = 0 = \delta_{\text{asynch}}$ to stabilize the asynchronous state with small E . The intrinsic parameters of the oscillators, namely K , β , and γ , are the same as those in Fig. 2(b). (b) The feedback parameters are set as $E = 1.1 \approx E_{\text{death}}$ and $\delta = -\pi/2 \approx \delta_{\text{death}}$ to induce the oscillation-death state with small E in the population that has the same parameters as Fig. 2(c).

$\theta_i(t)$ before and after the onset of the feedback. In Fig. 6(a), the feedback with the parameters $E = 0.3 \approx E_{\text{asynch}}$ and $\delta = 0 = \delta_{\text{asynch}}$ is applied at $t = 5050$, as marked by the black arrow. Upon the onset of the feedback, the population begins to be desynchronized, and r decreases with time. In Fig.6(b), the feedback parameters are chosen such that the oscillation-death state is induced with small feedback strength: $E = 1.10 \approx E_{\text{death}}$ and $\delta = -\pi/2 \approx \delta_{\text{death}}$. The figure indicates that the oscillations of the individual oscillators and the mean field terminate immediately because of the feedback.

V. INVESTIGATION ON THE ROBUSTNESS OF THE EFFECT OF FEEDBACK USING A DIFFERENT MODEL OF OSCILLATORS

Our analyses thus far are based on the model given by Eq. (6). As presented in Appendix A, this model is derived from a general class of coupled oscillator models. However, we assumed that coupling, inhomogeneity, and feedback are sufficiently weak to employ averaging approximations

and that the functions contain only the first harmonics. Furthermore, we assumed the natural frequencies to obey Lorentzian distribution to obtain the reduced dynamical equation given in Eq. (8). Here, to exemplify the robustness of the results to the violation of these assumptions, we provide numerical results for a model with the form given by Eq. (A5). Specifically, we consider

$$\dot{\theta}_i = 1 + \mu_i \cos \theta_i + \frac{K}{N} Z_v(\theta_i) \sum_{j=1}^N V(\theta_j) + E Z_f(\theta_i) f(\boldsymbol{\theta}). \quad (38)$$

We adopt the pulse-like signal $V(\theta) = \nu_n (1 + \cos \theta)^n$ used in [41], where n is the parameter on the sharpness of V , and $\nu_n = 2^n (n!)^2 / (2n)!$ normalizes $\int_0^{2\pi} V(\theta) d\theta$ to be 2π . We set $n = 10$. The phase sensitivity functions Z_v and Z_f are chosen to weakly include the second Fourier mode:

$$Z_v(\theta) = -\sin \theta + 0.2 \sin 2\theta, \quad (39)$$

$$Z_f(\theta) = \sin \theta + 0.2 \cos 2\theta. \quad (40)$$

Finally, μ_i is drawn from Gaussian distribution with mean 0 and standard deviation 0.1.

Numerical simulation of Eq. (38) is conducted to calculate $\langle R \rangle$ and $\langle \zeta \rangle$, which are shown in Fig. 7(a) and (b), respectively. These figures qualitatively agree with Fig. 4(a) and (d), suggesting the robustness of the results.

VI. CONCLUSION AND DISCUSSION

Motivated from the wide range of the applications of synchronization control, we analyzed an inhomogeneous population of phase oscillators exposed to global feedback. Detailed phase diagrams of the collective state are obtained based on the bifurcation analysis of the macroscopic equation derived using the Ott–Antonsen theory. The diagram displayed three types of macroscopic states, namely, the synchronously oscillating state, the asynchronous state, and the oscillation-death state. Exact and approximate optimizations of the feedback parameters for steering a synchronously oscillating population into the asynchronous or the oscillation-death state with minimum feedback strength are also presented. Although we assumed several conditions such as the weakness of the coupling and the feedback in the derivation of the model equation, the numerical investigation in Sec. V demonstrates that our results do not change qualitatively even when some of the assumptions are violated to some extent.

Herein, we focused on linear feedback F given by Eq. (2), and our extensive analysis revealed its utility for synchronization control. Linear feedback can be regarded as a basic methodology, and our study is expected to serve as a benchmark when more sophisticated feedback is to be designed.

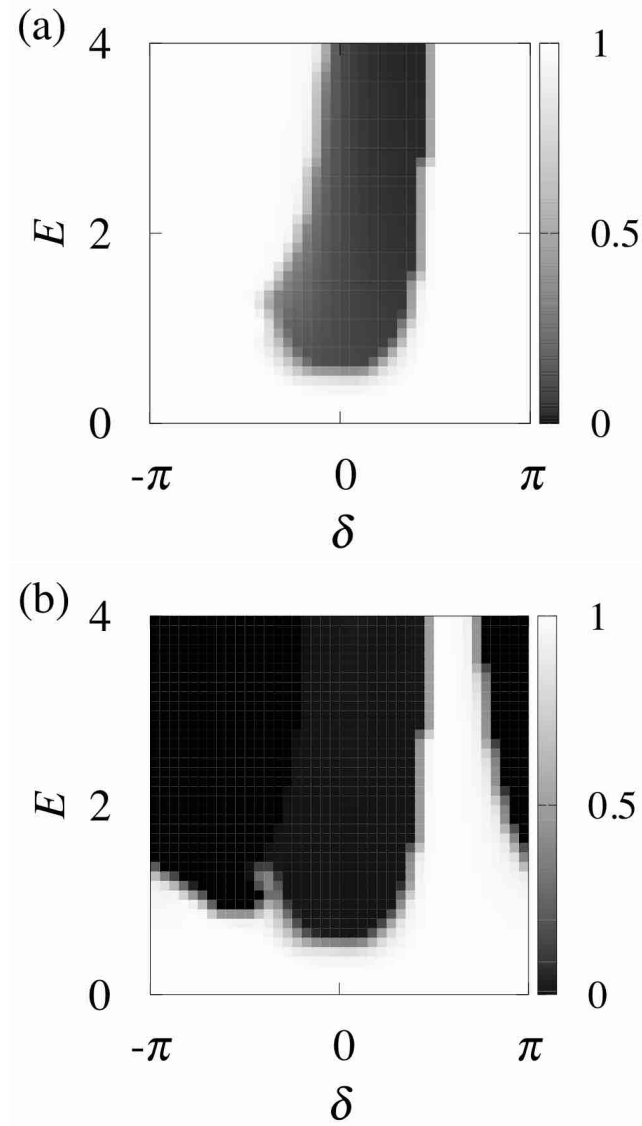


FIG. 7. Long-time average of (a) R and (b) ζ in the system of pulse-coupled oscillators under the feedback described by Eq. (38). Initial conditions are given by $\theta_i(0) = 2\pi(i-1)/N$.

A natural extension is to make the feedback function F nonlinear in R . Although it will not change the linear stability of the asynchronous state, it may alter the stability and the existence of other states in addition to the amplitude of the collective oscillation[42] A class of nonlinear feedback has been proposed in [23] for reducing the amplitude of the collective oscillation, and further investigated in successive studies [42–46]. In [47, 48], the authors showed that a class of delayed nonlinear feedback can stabilize complex dynamical states including a type of desynchronized state and demonstrated its ability to control electrochemical oscillators. Furthermore, regarding DBS, smooth feedback may not fulfill safety requirements[49]. In [28], the authors compare two types

of feedback: a smooth feedback and a series of pulses that are amplified according to the smooth feedback. They found that the pulses have a similar desynchronizing effect to the smooth feedback. The same approach might be applicable to the feedback studied in this article.

Our theoretical results can be demonstrated in some experimental systems. Recently, techniques for inferring phase dynamics and their interactions from observed oscillatory signals have been developed, and they have been utilized in experimental studies for predicting and controlling the dynamics of the oscillators [1, 34, 50–52]. These experiments have revealed various coupling and phase sensitivity functions; in some systems, the first Fourier component is dominant, while in other systems, some of the higher and the constant components are also prominent. In the former case, our analytical results may be verified quantitatively by estimating the values of ω_i , K , and β in Eq. (5) and implementing the global feedback loop. The feedback parameters δ and E can be tuned if R and Θ can be inferred online or two outputs from individual oscillators are available, as detailed in Appendix A.

Finally, we remark on the limitation of the current study. It should be noted that our results are based on phase oscillator models. A qualitatively different phase diagram may be obtained for limit-cycle oscillators whose amplitudes considerably deviate from that of the unperturbed periodic orbit. Therefore, to understand the effect of a large amplitude deviation on synchronization control, it is important to investigate models of limit-cycle oscillators and compare them with our results.

ACKNOWLEDGMENTS

The authors thank Kei-Ichi Ueda for helpful discussions on numerical bifurcation analysis. H.K. acknowledges the financial support from JSPS KAKENHI Grant No. 18K11464.

H.K. conceived the study and supervised the project. A.O. performed the analytical and numerical investigations. A.O. wrote the manuscript with support from H.K..

Appendix A: Derivation of our model given in Eq. (1)

We consider a general class of oscillator network given by

$$\dot{\mathbf{x}}_i = \mathbf{u}_i(\mathbf{x}_i; p_i, q_i), \tag{A1}$$

where $\mathbf{x}_i = (x_i, y_i, \dots)$ and \mathbf{u}_i ($i = 1, \dots, N$) are the state and the local vector field of the i th oscillator, respectively, and p_i and q_i are parameters. The interactions and external forcing are assumed to be given through variations in the parameters as $p_i = p_0 + \Delta p_i$ and $q_i = q_0 + \Delta q_i$,

where p_0 and q_0 are the parameter values common for all the oscillators and Δp_i and Δq_i describe perturbations. When we consider global coupling and feedback, the perturbations may be given as

$$\Delta p_i = \frac{K'}{N} \sum_{j=1}^N v(\mathbf{x}_i, \mathbf{x}_j), \quad (\text{A2})$$

$$\Delta q_i = \Delta q \equiv E' f(\mathbf{x}_1, \dots, \mathbf{x}_N), \quad (\text{A3})$$

where K' and E' are the strengths of coupling and feedback, respectively, and v and f are the functions describing coupling and feedback, respectively.

We follow the standard procedure of the phase reduction to obtain the corresponding phase description to Eq. (A1) [5, 53]. Let us introduce $\Delta \mathbf{u}_i(\mathbf{x}_i; p_i, q_i) = \mathbf{u}_i(\mathbf{x}_i; p_i, q_i) - \mathbf{u}(\mathbf{x}_i; p_i, q_i)$ for $i = 1, \dots, N$, which describes inhomogeneity in inherent oscillator properties. We assume that the unperturbed system, i.e.,

$$\dot{\mathbf{x}} = \mathbf{u}(\mathbf{x}; p_0, q_0), \quad (\text{A4})$$

has a stable limit cycle $\mathbf{x}^*(t)$. The phase of the unperturbed system is defined as a scalar field $\Phi(\mathbf{x})$ for the basin of attraction for the limit cycle such that the contour of $\Phi(\mathbf{x})$ describe the isochron of the unperturbed system[5, 54]. Using this scalar field, the phase of the i th oscillator is defined as $\theta_i = \Phi(\mathbf{x}_i(t))$ ($i = 1, \dots, N$).

We assume that the orbital stability of the cycle $\mathbf{x}^*(t)$ in the unperturbed system given by Eq. (A4) is sufficiently higher than perturbation strength. Then, to the lowest order in perturbations strengths, each phase obeys

$$\dot{\theta}_i = \omega + \mathbf{Z}(\theta_i) \cdot \mathbf{U}_i(\theta_i) + \frac{K'}{N} \sum_{j=1}^N Z_v(\theta_i) V(\theta_i, \theta_j) + E' Z_f(\theta_i) F(\boldsymbol{\theta}), \quad (\text{A5})$$

where ω is the natural frequency of the limit cycle \mathbf{x}^* ; \mathbf{U}_i, V, F are the parametric representations of $\Delta \mathbf{u}_i, v, f$ on the limit-cycle \mathbf{x}^* in terms of the phases, respectively; and \mathbf{Z}, Z_v, Z_f are the phase sensitivity functions, which can be expressed in terms of the derivatives of $\mathbf{u}(\mathbf{x}; p, q)$ and $\Phi(\mathbf{x})$. All the functions are 2π -periodic in each argument.

When the magnitudes of the perturbation terms, i.e., the second to fourth terms of the right-hand side in Eq. (A5), are sufficiently small compared to ω , we may further simplify the equation using an averaging approximation. The resultant equation is

$$\dot{\theta}_i = \omega + \Delta \omega_i + \frac{K'}{N} \sum_{j=1}^N \Gamma_v(\theta_i - \theta_j) + \frac{E'}{N} \sum_{j=1}^N \Gamma_f(\theta_i - \theta_j), \quad (\text{A6})$$

where the constant $\Delta\omega_i$ and the functions Γ_v and Γ_f can be expressed in terms of the functions appearing in Eq. (A5). If the last term in Eq. (A5) is not very small compared to ω , we can still average the other terms to obtain

$$\dot{\theta}_i = \omega + \Delta\omega_i + \frac{K'}{N} \sum_{j=1}^N \Gamma_v(\theta_i - \theta_j) + E' Z_f(\theta_i) F(\boldsymbol{\theta}). \quad (\text{A7})$$

In Eq. (A7), we may consider larger E' values than in Eq. (A6), which is the reason why we employ this type of model in this work.

Our model given in Eq. (1) is a version of Eq. (A7), where we assume that only the first harmonics are present in all the functions appearing in Eq. (A7); i.e., Γ_v , Z_f and F . This assumption is valid when we consider limit-cycle oscillators close to a Hopf bifurcation point, in which the phase sensitivity and the wave forms are well approximated by the functions with only the first harmonics and with the constant and first harmonics terms, respectively. Let us further assume that from each oscillator we can observe two quantities, such as $x_j(t)$ and $y_j(t)$. If we denote the trajectory of the unperturbed limit cycle $\mathbf{x}^*(t)$ by $\boldsymbol{\chi}(\Phi)$, i.e., $\boldsymbol{\chi}(\Phi(\mathbf{x}^*(t))) = \mathbf{x}^*(t)$, with its elements being $\boldsymbol{\chi} = (\chi_x, \chi_y, \dots)$, the variation of $\chi_x(\theta)$ and $\chi_y(\theta)$ are almost sinusoidal near the Hopf bifurcation point. Therefore, the unperturbed waveforms can be denoted by $\chi_x(\theta) \simeq \bar{\chi}_x + A_x \cos(\theta - \delta_x)$ and $\chi_y(\theta) \simeq \bar{\chi}_y + A_y \cos(\theta - \delta_y)$, where $\bar{\chi}_x$ and $\bar{\chi}_y$ are the average of $\chi_x(\theta)$ and $\chi_y(\theta)$, respectively, A_x and A_y are the oscillation amplitudes, and δ_x and δ_y are the phase offsets in the waveforms. We then give the feedback function f as

$$f = \sum_{j=1}^N \left[a \frac{x_j - \bar{x}_j}{A_x} + b \frac{y_j - \bar{y}_j}{A_y} \right], \quad (\text{A8})$$

where \bar{x}_j and \bar{y}_j denote the average values of x_j and y_j , respectively; and a and b are our control parameters. In the lowest order phase description, Eq. (A8) results in

$$F(\boldsymbol{\theta}) = \sum_{j=1}^N [a \cos(\theta_j - \delta_x) + b \cos(\theta_j - \delta_y)]. \quad (\text{A9})$$

We can further transform (A9) to

$$F(\boldsymbol{\theta}) = \mathcal{E} \sum_{j=1}^N \cos(\theta_j - \delta) \quad (\text{A10})$$

$$= \mathcal{E} R \cos(\Theta - \delta), \quad (\text{A11})$$

where

$$\mathcal{E} = \left[(a \cos \delta_x + b \cos \delta_y)^2 + (a \sin \delta_x + b \sin \delta_y)^2 \right]^{1/2}, \quad (\text{A12})$$

$$\tan \delta = \frac{a \sin \delta_x + b \sin \delta_y}{a \cos \delta_x + b \cos \delta_y}. \quad (\text{A13})$$

Therefore, we can give arbitrary \mathcal{E} and δ values by appropriately assigning a and b values. Because \tilde{E} in Eq. (1) is given by $\tilde{E} = E'\mathcal{E}$, we can also give an arbitrary \tilde{E} value.

Appendix B: Classification of the zero-eigenvalue bifurcation at the origin

The codimension-one bifurcation involving zero-eigenvalue at the origin is limited to the pitchfork bifurcation. One possible approach for this is to consider the facts that the saddle-node bifurcation may not occur because the constant solution $r = 0$ may not vanish in Eq. (8) and the pitchfork bifurcation rather than the transcritical bifurcation occurs because the symmetry of Eq. (8) implies that the emergence of a constant solution $r = r^* \neq 0$ must be accompanied with the emergence of $r = -r^*$ as well.

An alternative way is to perform the center manifold reduction[37], which will clarify that the bifurcation is actually the pitchfork one and whether the bifurcation is super- or sub-critical. Let the bifurcation parameter be $\mu = E - E_{\text{pf}}$, where E_{pf} is given by Eq. (16). Inserting $r = u + iv$ and $E = E_{\text{pf}} + \mu$ into Eq. (8), we obtain

$$\begin{pmatrix} \dot{u} \\ \dot{v} \end{pmatrix} = \begin{pmatrix} \Lambda - \frac{E_{\text{pf}} \cos \delta}{2} & -\Omega - \frac{E_{\text{pf}} \sin \delta}{2} \\ \Omega & \Lambda \end{pmatrix} \begin{pmatrix} u \\ v \end{pmatrix} + \begin{pmatrix} p(u, v) \\ q(u, v) \end{pmatrix}, \quad (\text{B1})$$

where

$$\begin{aligned} p(u, v) = & -\frac{\mu}{2}(u \cos \delta + v \sin \delta) + \frac{E_{\text{pf}} + \mu}{2}(u^2 - v^2)(u \cos \delta + v \sin \delta) \\ & - \frac{K}{2}(u^2 + v^2)(u \cos \beta + v \sin \beta), \end{aligned} \quad (\text{B2})$$

$$\begin{aligned} q(u, v) = & u^2 v [(E_{\text{pf}} + \mu) \cos \delta - \gamma - \Lambda] + uv^2 [(E_{\text{pf}} + \mu) \sin \delta + \Omega - 1] \\ & + u^3(\Omega - 1) + v^3(-\gamma - \Lambda). \end{aligned} \quad (\text{B3})$$

To reduce the system, let us transform the variables as follows:

$$\begin{pmatrix} u \\ v \end{pmatrix} = \begin{pmatrix} -\frac{\Lambda}{\Omega} & \frac{\Lambda \sin \delta + \Omega \cos \delta}{\Omega \sin \delta - \Lambda \cos \delta} \\ 1 & 1 \end{pmatrix} \begin{pmatrix} \hat{u} \\ \hat{v} \end{pmatrix}, \quad (\text{B4})$$

which yields

$$\begin{pmatrix} \dot{\hat{u}} \\ \dot{\hat{v}} \end{pmatrix} = \begin{pmatrix} 0 & 0 \\ 0 & \hat{\lambda} \end{pmatrix} \begin{pmatrix} \hat{u} \\ \hat{v} \end{pmatrix} + \begin{pmatrix} a_1 \mu \hat{u} + a_2 \mu \hat{v} + a_3 \hat{u}^3 + O(v^3, uv^2, u^2 v) \\ b \mu \hat{u} + O(\mu \hat{v}, \hat{v}^3, \hat{u} \hat{v}^2, \hat{u}^2 \hat{v}, \hat{u}^3) \end{pmatrix} \quad (\text{B5})$$

where

$$\hat{\lambda} = \frac{\cos \delta (\Lambda^2 - \Omega^2) - 2\Lambda\Omega \sin \delta}{\Lambda \cos \delta - \Omega \sin \delta}, \quad (\text{B6})$$

$$a_1 = \frac{(\Omega \sin \delta - \Lambda \cos \delta)^2}{2[(\Omega^2 - \Lambda^2) \cos \delta + 2\Lambda\Omega \sin \delta]}, \quad (\text{B7})$$

$$a_2 = \frac{\Omega^2}{2[(\Omega^2 - \Lambda^2) \cos \delta + 2\Lambda\Omega \sin \delta]}, \quad (\text{B8})$$

$$a_3 = \frac{(\Lambda^2 + \Omega^2) \{ (-2\gamma\Lambda\Omega + \Lambda^2 - \Omega^2) \sin \delta + [\gamma(\Lambda^2 - \Omega^2) + 2\Lambda\Omega] \cos \delta \}}{\Omega^2 [(\Omega^2 - \Lambda^2) \cos \delta + 2\Lambda\Omega \sin \delta]}, \quad (\text{B9})$$

$$b_1 = \frac{(\Lambda \cos \delta - \Omega \sin \delta)^2}{2(\Lambda^2 - \Omega^2) \cos \delta - 4\Lambda\Omega \sin(\delta)}. \quad (\text{B10})$$

The center manifold $\hat{v} = c(\hat{u}, \mu)$ up to the second order is given by

$$c(\hat{u}, \mu) = -\frac{b}{\hat{\lambda}} \mu \hat{u} + O(\hat{u} \mu^2, \hat{u}^3). \quad (\text{B11})$$

On this center manifold, the dynamics is reduced to

$$\dot{\hat{u}} = a_1 \mu \left(1 - \frac{a_2 b}{\hat{\lambda} a_1} \mu \right) \hat{u} + a_3 \hat{u}^3 + O(\mu \hat{u}^3, \mu^3 \hat{u}). \quad (\text{B12})$$

Equation (B12) implies that the pitchfork bifurcation occurs at $\mu = 0$. The origin changes its stability through this bifurcation when $\hat{\lambda} < 0$. It is supercritical for $a_3 < 0$ and subcritical for $a_3 > 0$.

Below, we show that the bifurcation is subcritical when $\hat{\lambda} < 0$, $\Omega > 0$, and E_{pf} is sufficiently small compared to Ω/γ . Because $E \geq 0$, and the numerator of E_{pf} is positive, the denominator of E_{pf} is also positive:

$$\Lambda \cos \delta - \Omega \sin \delta > 0, \quad (\text{B13})$$

which implies that the denominator of $\hat{\lambda}$ is positive. Thus, if $\hat{\lambda} < 0$, the numerator of $\hat{\lambda}$ is negative, i.e.,

$$(\Lambda^2 - \Omega^2) \cos \delta - 2\Lambda\Omega \sin \delta < 0. \quad (\text{B14})$$

Under this condition, a_3 is positive if

$$(\gamma(\Lambda^2 - \Omega^2) + 2\Lambda\Omega) \cos \delta > (2\gamma\Lambda\Omega - \Lambda^2 + \Omega^2) \sin \delta \quad (\text{B15})$$

$$\iff \Omega(\Lambda \cos \delta - \Omega \sin \delta) > -\Lambda(\Lambda \sin \delta + \Omega \cos \delta) + \gamma[2\Lambda\Omega \sin \delta - (\Lambda^2 - \Omega^2) \cos \delta] \quad (\text{B16})$$

We first consider the case of $\Lambda \geq 0$. Then, the first term of the right-hand side of Eq. (B16) is negative because Eqs. (B13) and (B14) yield

$$0 \leq \Lambda(\Lambda \cos \delta - \Omega \sin \delta) < \Omega(\Lambda \sin \delta + \Omega \cos \delta). \quad (\text{B17})$$

As for the second term, noting that $|\cos \delta|, |\sin \delta| \leq 1$, we obtain

$$2\Lambda\Omega \sin \delta - (\Lambda^2 - \Omega^2) \cos \delta \leq 2\Lambda\Omega + \Lambda^2 + \Omega^2 \leq 2(\Lambda^2 + \Omega^2) \quad (\text{B18})$$

Equations (B16), (B17), and (B18) yield the following sufficient condition for a_3 to be positive:

$$\Omega(\Lambda \cos \delta - \Omega \sin \delta) > 2\gamma(\Lambda^2 + \Omega^2), \quad (\text{B19})$$

which is equivalent to

$$E_{\text{pf}} = \frac{2(\Lambda^2 + \Omega^2)}{\Lambda \cos \delta - \Omega \sin \delta} < \frac{\Omega}{\gamma}. \quad (\text{B20})$$

Therefore, for $\Lambda \geq 0$, the bifurcation is subcritical when E_{pf} is sufficiently small compared to Ω/γ .

We next consider the case of $\Lambda < 0$. If $\Lambda \sin \delta + \Omega \cos \delta < 0$ holds, we can derive Eq. (B20) in the same manner as the case of $\Lambda \geq 0$. When $\Lambda \sin \delta + \Omega \cos \delta \geq 0$, we evaluate the right-hand side of Eq. (B16) as follows. As $|\Lambda| < \gamma$ holds for $\Lambda < 0$,

$$-\Lambda(\Lambda \sin \delta + \Omega \cos \delta) < \gamma(|\Lambda| + \Omega). \quad (\text{B21})$$

This equation and Eqs. (B16) and (B18) yield the sufficient condition for the subcritical bifurcation

$$\Omega(\Lambda \cos \delta - \Omega \sin \delta) > 2\gamma(\Lambda^2 + \Omega^2) \left(1 + \frac{|\Lambda| + \Omega}{2(\Lambda^2 + \Omega^2)}\right), \quad (\text{B22})$$

which is equivalent to

$$E_{\text{pf}} < \frac{\Omega}{\gamma \left(1 + \frac{|\Lambda| + \Omega}{2(\Lambda^2 + \Omega^2)}\right)}. \quad (\text{B23})$$

From Eq.(B20) and Eq.(B23), it is shown that the pitchfork bifurcation is subcritical if E_{pf} is sufficiently small compared to Ω/γ .

Near the parameter regions considered in Fig. 2, E_{pf} is small enough, and hence the pitchfork bifurcation involving a stable fixed point is subcritical.

Appendix C: Weakly nonlinear analysis of the Hopf bifurcation

We show below that the Hopf bifurcation at the origin is always supercritical. Substituting $r = u + iv$ and the value of the feedback strength at the bifurcation point, given by Eq. (14), into Eq. (8), we have

$$\begin{pmatrix} \dot{u} \\ \dot{v} \end{pmatrix} = \begin{pmatrix} -\Lambda & -2\Lambda \tan \delta - \Omega \\ \Omega & \Lambda \end{pmatrix} \begin{pmatrix} u \\ v \end{pmatrix} + \begin{pmatrix} g(u, v) \\ h(u, v) \end{pmatrix}, \quad (\text{C1})$$

where

$$g(x, y) = 2\Lambda (x^2 - y^2) (x + y \tan \delta) - \frac{K}{2} (x^2 + y^2) (x \cos \beta + y \sin \beta), \quad (\text{C2})$$

$$h(x, y) = \frac{K}{2} (x^2 + y^2) (x \sin \beta - y \cos \beta) + 4\Lambda xy(x + y \tan \delta) \quad (\text{C3})$$

To simplify the calculation, we change the coordinates to

$$\begin{pmatrix} \tilde{u} \\ \tilde{v} \end{pmatrix} = \begin{pmatrix} \Omega/\tilde{\omega} & \Lambda/\tilde{\omega} \\ 0 & 1 \end{pmatrix} \begin{pmatrix} u \\ v \end{pmatrix}, \quad (\text{C4})$$

where $\tilde{\omega} = \sqrt{-\Lambda^2 + \Omega^2 + 2\Lambda\Omega \tan \delta}$. Then, \tilde{u} and \tilde{v} obey

$$\begin{pmatrix} \dot{\tilde{u}} \\ \dot{\tilde{v}} \end{pmatrix} = \begin{pmatrix} 0 & -\tilde{\omega} \\ \tilde{\omega} & 0 \end{pmatrix} \begin{pmatrix} \tilde{u} \\ \tilde{v} \end{pmatrix} + \begin{pmatrix} \tilde{g}(\tilde{u}, \tilde{v}) \\ \tilde{h}(\tilde{u}, \tilde{v}) \end{pmatrix}, \quad (\text{C5})$$

where

$$\begin{pmatrix} \tilde{g}(\tilde{u}, \tilde{v}) \\ \tilde{h}(\tilde{u}, \tilde{v}) \end{pmatrix} = \begin{pmatrix} \Omega/\tilde{\omega} & \Lambda/\tilde{\omega} \\ 0 & 1 \end{pmatrix} \begin{pmatrix} g(u(\tilde{u}, \tilde{v}), v(\tilde{u}, \tilde{v})) \\ h(u(\tilde{u}, \tilde{v}), v(\tilde{u}, \tilde{v})) \end{pmatrix}. \quad (\text{C6})$$

Then, $z = u + iv$ obeys

$$\dot{z} = i\tilde{\omega}z + \tilde{g} + i\tilde{h}. \quad (\text{C7})$$

Using a near-identity transformation, Equation (C7) is further reduced to the following normal form of the Hopf bifurcation [37]

$$\dot{w} = i\tilde{\omega}w + d|w|^2 \bar{w} + O(|w|^5), \quad (\text{C8})$$

where $w, d \in \mathbb{C}$, and

$$\text{Re}(d) = -\gamma \left(1 + \frac{\Lambda}{\Omega} \tan \delta \right). \quad (\text{C9})$$

The bifurcation is supercritical when $\text{Re}(d) < 0$. Noting that $\gamma > 0$, we may further show $\text{Re}(d) < 0$ as follows. When $\frac{\Lambda}{\Omega} \tan \delta \geq 0$, it is obvious that $\text{Re}(d) < 0$ from Eq. (C9). When $\frac{\Lambda}{\Omega} \tan \delta < 0$, the following inequality holds:

$$1 + \frac{\Lambda}{\Omega} \tan \delta > 1 + 2\frac{\Lambda}{\Omega} \tan \delta. \quad (\text{C10})$$

Moreover, Eq. (15) implies that the Hopf bifurcation at the origin occurs only when

$$-\Lambda^2 + \Omega^2 + 2\Lambda\Omega \tan \delta > 0. \quad (\text{C11})$$

From Eqs. (C10) and (C11), we have

$$1 + \frac{\Lambda}{\Omega} \tan \delta > \left(\frac{\Lambda}{\Omega} \right)^2 > 0 \quad (\text{C12})$$

and hence $\text{Re}(d) < 0$. Therefore, the Hopf bifurcation at the origin is supercritical for any parameter values.

Appendix D: Derivation of the sufficient condition for a nonzero fixed point

Here, under the conditions $K > 2K_c$ and $\Omega' = 1 + K \sin \beta > 0$, we derive Eqs. (26) and (27), i.e., a sufficient condition for Eq. (18) to have a nonzero fixed point. Note that an intersection of the two nullclines

$$-\gamma + (1 - R^2) \left[\frac{K}{2} \cos \beta - \frac{E}{4} (\cos(\delta - 2\Theta) + \cos \delta) \right] = 0 \quad (\text{D1})$$

and

$$1 + (1 + R^2) \left[\frac{K}{2} \sin \beta + \frac{E}{4} (\sin \delta - \sin(\delta - 2\Theta)) \right] = 0 \quad (\text{D2})$$

gives a nonzero fixed point. Thus there exists a fixed point (R^*, Θ^*) such that $R_{\text{lower}} < R^* < 1$ if both of the following conditions are satisfied: (i) the nullcline given by Eq. (D1) is defined for any Θ , and the value of R on the nullcline always satisfies $R_{\text{lower}} < R^* < 1$, and (ii) the nullcline given by Eq. (D2) passes through the region $R_{\text{lower}} < R^* < 1$ on the R - Θ plane.

The first condition is equivalent to that the following inequality holds for any Θ :

$$R_{\text{lower}}^2 < 1 - \frac{4\gamma}{2K \cos \beta - E [\cos(\delta - 2\Theta) + \cos \delta]} < 1, \quad (\text{D3})$$

which is satisfied when

$$E < \frac{2K \cos \beta - 4\gamma (1 - R_{\text{lower}}^2)^{-1}}{1 + \cos \delta}. \quad (\text{D4})$$

Next we discuss the second condition. Equation (D2) yields $R^2 = -1 + S(\sin(\delta - 2\Theta))^{-1}$, where

$$S(x) = -\frac{K}{2} \sin \beta + \frac{E}{4} (x - \sin \delta) \quad (\text{D5})$$

is a monotonically increasing function of x . Because $\sin(\delta - 2\Theta)$ is in the range of $[1, 1]$, the nullcline given by Eq. (D2) crosses over the region $R_{\text{lower}} < R^* < 1$ if

$$S(-1) < \frac{1}{2} \quad (\text{D6})$$

and

$$S(1) > (1 + R_{\text{lower}}^2)^{-1}. \quad (\text{D7})$$

When $\Omega' > 0$, the inequality given by (D6) holds for any $E \geq 0$. In contrast, inequality (D7) holds when

$$E > E_{\text{lower}} \left[1 + \frac{1 - R_{\text{lower}}^2}{(1 + R_{\text{lower}}^2)(1 + K \sin \beta)} \right], \quad (\text{D8})$$

where E_{lower} is given by Eq. (24).

Therefore, if Eqs. (D4) and (D8) are satisfied, a nonzero fixed point (R^*, Θ^*) that satisfies $R_{\text{lower}} < R^* < 1$ exists. As a special case, we obtain Eqs. (26) and (27), respectively, by setting $R_{\text{lower}} = \sqrt{1 - \frac{2K_c}{K}}$ in Eqs. (D8) and (D4).

We can find a value of E that satisfies both of Eqs. (26) and (27) when

$$E_{\text{lower}} (1 + \eta) < \frac{K \cos \beta}{1 + \cos \delta}, \quad (\text{D9})$$

which is equivalent to

$$\frac{2}{1 - \sin \delta} \left[\frac{1}{K - K_c} + \sin \beta \right] - \frac{\cos \beta}{1 + \cos \delta} < 0. \quad (\text{D10})$$

Equation (D10) holds when $\beta \simeq 0$ and K is sufficiently large for a given value of δ .

Appendix E: Analysis on the codimension-two bifurcation point

By imposing $\text{Tr } L = |L| = 0$, we obtain the values of the feedback parameters at which the Hopf bifurcation curve (14) and the pitchfork bifurcation curve (16) meet as

$$\sin \delta = \frac{\Omega}{|\Omega|} \frac{\Lambda^2 - \Omega^2}{\Lambda^2 + \Omega^2}, \quad (\text{E1})$$

$$\cos \delta = \frac{2\Lambda}{\Lambda^2 + \Omega^2} \frac{|\Omega|}{\Lambda}, \quad (\text{E2})$$

$$E = \frac{2(\Lambda^2 + \Omega^2)}{|\Omega|}. \quad (\text{E3})$$

Substituting $r = u + iv$ together with Eq. (E1)–(E3) into Eq. (8), we have

$$\begin{pmatrix} \dot{u} \\ \dot{v} \end{pmatrix} = \begin{pmatrix} -\Lambda & -\frac{\Lambda^2}{\Omega} \\ \Omega & \Lambda \end{pmatrix} \begin{pmatrix} u \\ v \end{pmatrix} + \begin{pmatrix} g_2(u, v) \\ h_2(u, v) \end{pmatrix}, \quad (\text{E4})$$

where

$$g_2(u, v) = (\Lambda - \gamma)u^3 + \left(1 - 2\Omega + \frac{\Lambda^2}{\Omega}\right)u^2v - (\gamma + 3\Lambda)uv^2 + \left(1 - \frac{\Lambda^2}{\Omega}\right)v^3, \quad (\text{E5})$$

$$h_2(u, v) = (\Omega - 1)u^3 - (\gamma - 3\Lambda)u^2v + \left(-1 - \Omega + \frac{2\Lambda^2}{\Omega}\right)uv^2 - (\gamma + \Lambda)v^3. \quad (\text{E6})$$

Next, we transform the linear part into the Jordan normal form by the following change of variables:

$$\begin{pmatrix} \check{u} \\ \check{v} \end{pmatrix} = \begin{pmatrix} 0 & 1 \\ \Omega & \Lambda \end{pmatrix} \begin{pmatrix} u \\ v \end{pmatrix}, \quad (\text{E7})$$

which yields

$$\begin{pmatrix} \dot{\check{u}} \\ \dot{\check{v}} \end{pmatrix} = \begin{pmatrix} \check{v} \\ 0 \end{pmatrix} + \begin{pmatrix} c_1 \check{u}^3 + c_2 \check{u}^2 \check{v} + c_3 \check{u} \check{v}^2 + c_4 \check{v}^3 \\ d_1 \check{u}^3 + d_2 \check{u}^2 \check{v} + d_3 \check{u} \check{v}^2 + d_4 \check{v}^3 \end{pmatrix}, \quad (\text{E8})$$

where

$$c_1 = (\Lambda^2 + \Omega^2) (\Lambda - \gamma\Omega) / \Omega^3, \quad (\text{E9})$$

$$c_2 = (2\gamma\Lambda\Omega - \Lambda^2\Omega - 3\Lambda^2 - \Omega^2 - \Omega^3) / \Omega^3, \quad (\text{E10})$$

$$c_3 = (3\Lambda - \gamma\Omega) / \Omega^3, \quad (\text{E11})$$

$$c_4 = (-1 + \Omega) / \Omega^3, \quad (\text{E12})$$

$$d_1 = (\Lambda^2 + \Omega^2)^2 / \Omega^3, \quad (\text{E13})$$

$$d_2 = (\Lambda^2 + \Omega^2) (-\gamma\Omega - 3\Lambda) / \Omega^3, \quad (\text{E14})$$

$$d_3 = [(3\Lambda^2 + \Omega^2) - 2\Omega(-\gamma\Lambda + \Lambda^2 + \Omega^2)] / \Omega^3, \quad (\text{E15})$$

$$d_4 = [-\Lambda - \Omega(\gamma - 2\Lambda)] / \Omega^3. \quad (\text{E16})$$

Equation (E8) is then reduced to

$$\begin{pmatrix} \dot{U} \\ \dot{V} \end{pmatrix} = \begin{pmatrix} V \\ 0 \end{pmatrix} + \begin{pmatrix} 0 \\ d_1 U^3 + (3c_1 + d_2) U^2 V \end{pmatrix} + O(U^5, U^4 V, U^3 V^2, U^2 V^3, UV^4, V^5) \quad (\text{E17})$$

by the following near-identity transformation

$$\begin{pmatrix} \check{u} \\ \check{v} \end{pmatrix} = \begin{pmatrix} U \\ V \end{pmatrix} + \begin{pmatrix} \frac{1}{6}(2c_2 + d_3) U^3 + \frac{1}{2}(c_3 + d_4) U^2 V + c_4 UV^2 \\ -c_1 U^3 + \frac{1}{2} d_3 U^2 V + d_4 UV^2 \end{pmatrix}. \quad (\text{E18})$$

The signs of d_1 and $d'_2 := 3c_1 + d_2 = -4\gamma(\Lambda^2 + \Omega^2) / \Omega^2$ determine the types of the codimension-one bifurcation that occurs near the codimension-two bifurcation point[37]. The heteroclinic bifurcation as well as the Hopf and the pitchfork bifurcations occurs for $d_1 d'_2 < 0$, while the bifurcation involving a pair of homoclinic orbit occurs for $d_1 d'_2 > 0$ [37]. The former is the case for $\Omega > 0$, and the latter is the case for $\Omega < 0$.

Note that the analysis above only gives the information around a specific codimension-two bifurcation point and does not necessarily imply that the Hopf bifurcation involving nonzero fixed point may not occur for $\Omega > 0$. In practice, we numerically observed it for some parameter sets even when $\Omega > 0$.

Appendix F: Numerical search for limit-cycle solutions of Eq. (8)

While the bifurcation analyses in Sec. III is comprehensive in regard to the local bifurcations, some global bifurcations such as saddle–node bifurcation of periodic orbits are not considered there. These global bifurcations might create or destroy stable limit cycles, affecting the stability region of the synchronously oscillating state in Fig. 1.

Thus, we numerically verified that the stability boundary of the synchronously oscillating state consists of the Hopf, SNIC, and heteroclinic bifurcation curves obtained in Sec. III as detailed below. For each parameter set, 100 initial conditions for $\text{Re}(r)$ and $\text{Im}(r)$ are drawn from uniform distribution on the unit disk, and the type of the attractor to which each orbit converges is detected. In the black region in Fig. 8, at least one orbit converges to a limit cycle. The edge of the black region agrees with the bifurcation curves that are inferred to form the stability boundary of the collective oscillation.

The type of the attractor is classified according to the following criteria. (i) Let Δr_t be the norm of the variation of the orbit between time t and $t + \Delta t$, where $\Delta t = 0.01$. The orbit is considered to be converged to a fixed point if the phase point is moving slowly ($\Delta r_t, \Delta r_{t-\Delta t}, \Delta r_{t-2\Delta t} < 10^{-5}$) and is slowing exponentially ($|\Delta r_t/\Delta r_{t-\Delta t} - \Delta r_{t-\Delta t}/\Delta r_{t-2\Delta t}| < 10^{-5}$). (ii) Let x_{\max} and x_{\min} be the maximum and the minimum, respectively, of $\text{Re}(r)$ during an interval ($10000 < t < 20000$). Then, let y_n be the n th intersection of the line $\text{Re}(r) = (x_{\max} + x_{\min})/2$ and the orbit that transverses the line with $\text{Re}(\dot{r}) > 0$. The orbit is considered to be converged to a limit cycle when $|y_n - y_{n-1}| < 10^{-5}$. With this criteria, we conclude that every orbit is converged to either a fixed point or a limit cycle.

-
- [1] A Pikovsky, M Rosenblum, and J Kurths. *Synchronization: A Universal Concept in Nonlinear Sciences*. 2001.
 - [2] Leon Glass. Synchronization and rhythmic processes in physiology. *Nature*, 410(6825):277–284, 2001.
 - [3] Alex Arenas, Albert Díaz-Guilera, Jurgen Kurths, Yamir Moreno, and Changsong Zhou. Synchronization in complex networks. *Phys. Rep.*, 469(3):93 – 153, 2008.
 - [4] A T Winfree. *The Geometry of Biological Time*. Springer, New York, 2nd edition, 2001.
 - [5] Y Kuramoto. *Chemical Oscillations, Waves, and Turbulence*. Springer, New York, 1984.
 - [6] Adilson E Motter, Seth A Myers, Marian Anghel, and Takashi Nishikawa. Spontaneous synchrony in power-grid networks. *Nat. Phys.*, 9(3):191–197, 2013.
 - [7] J T Enright. Temporal precision in circadian systems: a reliable neuronal clock from unreliable com-

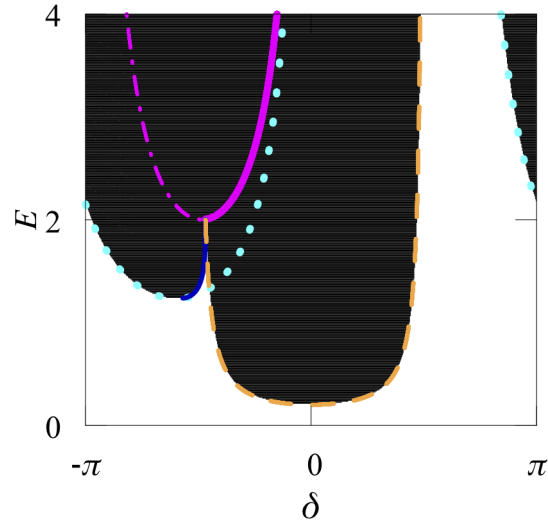


FIG. 8. (Color online) The stable region of the limit cycle solution. The region where at least one stable limit cycle exists is filled with black. The bifurcation curves obtained in Sec. III are also plotted. The Hopf, SNIC, and heteroclinic bifurcation curves agree with the boundary of the black region.

ponents? *Science (80-.)*, 209(4464):1542–1545, sep 1980.

- [8] Erik D Herzog, Sara J Aton, Rika Numano, Yoshiyuki Sakaki, and Hajime Tei. Temporal Precision in the Mammalian Circadian System: A Reliable Clock from Less Reliable Neurons. *J. Biol. Rhythms*, 19(1):35–46, feb 2004.
- [9] Daniel J Needleman, Paul H E Tiesinga, and Terrence J Sejnowski. Collective enhancement of precision in networks of coupled oscillators. *Phys. D Nonlinear Phenom.*, 155(3-4):324–336, 2001.
- [10] Hiroshi Kori, Yoji Kawamura, and Naoki Masuda. Structure of cell networks critically determines oscillation regularity. *J. Theor. Biol.*, 297:61–72, 2012.
- [11] Auke Jan Ijspeert. Central pattern generators for locomotion control in animals and robots: A review. *Neural Networks*, 21(4):642–653, 2008.
- [12] Stefan Lämmer, Hiroshi Kori, Karsten Peters, and Dirk Helbing. Decentralised control of material or traffic flows in networks using phase-synchronisation. *Phys. A Stat. Mech. its Appl.*, 363(1):39–47, 2006.
- [13] D R ALEKO and S Djahel. An IoT Enabled Traffic Light Controllers Synchronization Method for Road Traffic Congestion Mitigation. In *2019 IEEE Int. Smart Cities Conf.*, pages 709–715, 2019.
- [14] Steven H Strogatz, Daniel M Abrams, Allan McRobie, Bruno Eckhardt, and Edward Ott. Crowd synchrony on the Millennium Bridge. *Nature*, 438(7064):43–44, 2005.
- [15] Constance Hammond, Hagai Bergman, and Peter Brown. Pathological synchronization in Parkinson’s disease: networks, models and treatments. *Trends Neurosci.*, 30(7):357–364, 2007.
- [16] Matthew M McGregor and Alexandra B Nelson. Circuit Mechanisms of Parkinson’s Disease. *Neuron*, 101(6):1042–1056, 2019.

- [17] Melissa J Armstrong and Michael S Okun. Diagnosis and Treatment of Parkinson Disease: A Review. *JAMA*, 323(6):548–560, feb 2020.
- [18] Patricia Limousin and Tom Foltynie. Long-term outcomes of deep brain stimulation in Parkinson disease. *Nat. Rev. Neurol.*, 15(4):234–242, 2019.
- [19] Jeff M Bronstein, Michele Tagliati, Ron L Alterman, Andres M Lozano, Jens Volkmann, Alessandro Stefani, Fay B Horak, Michael S Okun, Kelly D Foote, Paul Krack, Rajesh Pahwa, Jaimie M Henderson, Marwan I Hariz, Roy A Bakay, Ali Rezai, William J Marks Jr, Elena Moro, Jerrold L Vitek, Frances M Weaver, Robert E Gross, and Mahlon R DeLong. Deep Brain Stimulation for Parkinson Disease: An Expert Consensus and Review of Key Issues. *Arch. Neurol.*, 68(2):165, feb 2011.
- [20] Minseok Kim, Matthias Bertram, Michael Pollmann, Alexander von Oertzen, Alexander S Mikhailov, Harm Hinrich Rotermund, and Gerhard Ertl. Controlling Chemical Turbulence by Global Delayed Feedback: Pattern Formation in Catalytic CO Oxidation on Pt(110). *Science (80-.)*, 292(5520):1357 – 1360, may 2001.
- [21] Michael Rosenblum and Arkady Pikovsky. Delayed feedback control of collective synchrony: An approach to suppression of pathological brain rhythms. *Phys. Rev. E*, 70(4):041904, oct 2004.
- [22] Michael G Rosenblum and Arkady S Pikovsky. Controlling Synchronization in an Ensemble of Globally Coupled Oscillators. *Phys. Rev. Lett.*, 92(11):114102, mar 2004.
- [23] Oleksandr V Popovych, Christian Hauptmann, and Peter A Tass. Effective Desynchronization by Nonlinear Delayed Feedback. *Phys. Rev. Lett.*, 94(16):164102, apr 2005.
- [24] Irmantas Ratas and Kestutis Pyragas. Controlling synchrony in oscillatory networks via an act-and-wait algorithm. *Phys. Rev. E - Stat. Nonlinear, Soft Matter Phys.*, 90(3):32914, sep 2014.
- [25] Natalia Tukhlina, Michael Rosenblum, Arkady Pikovsky, and Jürgen Kurths. Feedback suppression of neural synchrony by vanishing stimulation. *Phys. Rev. E*, 75(1):011918, jan 2007.
- [26] Ming Luo, Yongjun Wu, and Jianhua Peng. Washout filter aided mean field feedback desynchronization in an ensemble of globally coupled neural oscillators. *Biol. Cybern.*, 101(3):241–246, 2009.
- [27] Alessio Franci, Antoine Chaillet, Elena Panteley, and Françoise Lamnabhi-Lagarrigue. Desynchronization and inhibition of Kuramoto oscillators by scalar mean-field feedback. *Math. Control. Signals, Syst.*, 24(1):169–217, 2012.
- [28] Oleksandr V Popovych, Borys Lysyansky, Michael Rosenblum, Arkady Pikovsky, and Peter A Tass. Pulsatile desynchronizing delayed feedback for closed-loop deep brain stimulation. *PLoS One*, 12(3):e0173363, mar 2017.
- [29] Shijie Zhou, Peng Ji, Qing Zhou, Jianfeng Feng, Jürgen Kurths, and Wei Lin. Adaptive elimination of synchronization in coupled oscillator. *New J. Phys.*, 19(8):083004, 2017.
- [30] Aneta Koseska, Evgeny Volkov, and Jürgen Kurths. Oscillation quenching mechanisms: Amplitude vs. oscillation death. *Phys. Rep.*, 531(4):173–199, 2013.
- [31] Edward Ott and Thomas M Antonsen. Low dimensional behavior of large systems of globally coupled oscillators. *Chaos An Interdiscip. J. Nonlinear Sci.*, 18(3):037113, sep 2008.

- [32] Edward Ott and Thomas M Antonsen. Long time evolution of phase oscillator systems. *Chaos An Interdiscip. J. Nonlinear Sci.*, 19(2):023117, may 2009.
- [33] Peter Ashwin, Stephen Coombes, and Rachel Nicks. Mathematical Frameworks for Oscillatory Network Dynamics in Neuroscience. *J. Math. Neurosci.*, 6(1):2, 2016.
- [34] Tomislav Stankovski, Tiago Pereira, Peter V. E. McClintock, and Aneta Stefanovska. Coupling functions: Universal insights into dynamical interaction mechanisms. *Rev. Mod. Phys.*, 89(4):045001, nov 2017.
- [35] Hidetsugu Sakaguchi and Yoshiki Kuramoto. A Soluble Active Rotater Model Showing Phase Transitions via Mutual Entertainment. *Prog. Theor. Phys.*, 76(3):576–581, sep 1986.
- [36] Ken H Nagai and Hiroshi Kori. Noise-induced synchronization of a large population of globally coupled nonidentical oscillators. *Phys. Rev. E*, 81(6):065202, jun 2010.
- [37] J Guckenheimer and P Holmes. *Nonlinear Oscillations, Dynamical Systems, and Bifurcations of Vector Fields*. Springer-Verlag, 1983.
- [38] Bard Ermentrout. *Simulating, analyzing, and animating dynamical systems: a guide to XPPAUT for researchers and students*. SIAM, 2002.
- [39] Lauren M Childs and Steven H Strogatz. Stability diagram for the forced Kuramoto model. *Chaos An Interdiscip. J. Nonlinear Sci.*, 18(4):43128, dec 2008.
- [40] H Daido. Scaling behaviour at the onset of mutual entrainment in a population of interacting oscillators. *J. Phys. A. Math. Gen.*, 20(10):L629–L636, 1987.
- [41] Joel T Ariaratnam and Steven H Strogatz. Phase Diagram for the Winfree Model of Coupled Nonlinear Oscillators. *Phys. Rev. Lett.*, 86(19):4278–4281, may 2001.
- [42] Denis S Goldobin and Arkady Pikovsky. Effects of Delayed Feedback on Kuramoto Transition. *Prog. Theor. Phys. Suppl.*, 161:43–52, jan 2006.
- [43] Oleksandr V Popovych, Christian Hauptmann, and Peter A Tass. Control of Neuronal Synchrony by Nonlinear Delayed Feedback. *Biol. Cybern.*, 95(1):69–85, 2006.
- [44] Oleksandr V Popovych and Peter A Tass. Multisite Delayed Feedback for Electrical Brain Stimulation , 2018.
- [45] Xiaohan Zhang and Shenquan Liu. Nonlinear delayed feedback control of synchronization in an excitatory–inhibitory coupled neuronal network. *Nonlinear Dyn.*, 96(4):2509–2522, 2019.
- [46] Oleksandr V Popovych, Christian Hauptmann, and Peter A Tass. Impact of Nonlinear Delayed Feedback on Synchronized Oscillators. *J. Biol. Phys.*, 34(3):267–279, 2008.
- [47] István Z Kiss, Craig G Rusin, Hiroshi Kori, and John L Hudson. Engineering Complex Dynamical Structures: Sequential Patterns and Desynchronization. *Science (80-.)*, 316(5833):1886 – 1889, jun 2007.
- [48] Hiroshi Kori, Craig G Rusin, István Z Kiss, and John L Hudson. Synchronization engineering: Theoretical framework and application to dynamical clustering. *Chaos An Interdiscip. J. Nonlinear Sci.*, 18(2):026111, jun 2008.

- [49] Daniel R Merrill, Marom Bikson, and John G R Jefferys. Electrical stimulation of excitable tissue: design of efficacious and safe protocols. *J. Neurosci. Methods*, 141(2):171–198, 2005.
- [50] István Z Kiss, Yumei Zhai, and John L Hudson. Predicting Mutual Entrainment of Oscillators with Experiment-Based Phase Models. *Phys. Rev. Lett.*, 94(24):248301, jun 2005.
- [51] Hiroshi Kori, Yoshiki Kuramoto, Swati Jain, István Z Kiss, and John L Hudson. Clustering in globally coupled oscillators near a Hopf bifurcation: Theory and experiments. *Phys. Rev. E*, 89(6):62906, jun 2014.
- [52] D Iatsenko, P V E McClintock, and A Stefanovska. Extraction of instantaneous frequencies from ridges in time–frequency representations of signals. *Signal Processing*, 125:290–303, 2016.
- [53] Yasuaki Kobayashi and Hiroshi Kori. Design principle of multi-cluster and desynchronized states in oscillatory media via nonlinear global feedback. *New J. Phys.*, 11(3):33018, 2009.
- [54] Arthur T Winfree. Biological rhythms and the behavior of populations of coupled oscillators. *J. Theor. Biol.*, 16(1):15–42, 1967.